



universität
wien

MASTERARBEIT

Titel der Masterarbeit

Microstructures and Mineralogy of Deformation Bands in Drill
Cores from the Matzen Hydrocarbon Reservoir, Austria

Verfasserin

Jasmin-Corin Kaiser, Bakk. rer. nat.

angestrebter akademischer Grad

Master of Science (M.Sc.)

Wien, 2011

Studienkennzahl lt. Studienblatt: A 066 815

Studienrichtung lt. Studienblatt: Masterstudium Erdwissenschaften

Betreuer: Mag. Dr. Ulrike Exner

Ao. Univ.-Prof. Mag. Dr. Susanne Gier

TABLE OF CONTENTS

TABLE OF CONTENTS.....	2
ABSTRACT.....	4
ZUSAMMENFASSUNG	6
INTRODUCTION.....	8
GEOLOGICAL SETTING	10
MATZEN FIELD	13
SAMPLES AND METHODS	15
SAMPLES	15
METHODS	17
<i>Optical Microscopy.....</i>	<i>17</i>
<i>X-Ray Diffraction (XRD).....</i>	<i>17</i>
<i>Scanning Electron Microscopy (SEM).....</i>	<i>17</i>
<i>Electron Microprobe Analysis.....</i>	<i>18</i>
<i>Cathodoluminescence (CL).....</i>	<i>18</i>
<i>Carbon and Oxygen Stable Isotope Analyses.....</i>	<i>18</i>
RESULTS.....	20
LITHOLOGY	21
DIAGENETIC PROCESSES	24
MICROSTRUCTURES	28
DISCUSSION	32
CONCLUSIONS	34
REFERENCES.....	35
ADDITIONAL RESULTS	40

ACKNOWLEDGMENT47

CURRICULUM VITAE48

Abstract

In porous sedimentary rocks, fault zones are frequently accompanied by deformation bands. These tabular zones of displacement indicate predominant grain rotation and in many cases grain fracturing. These mechanisms often result in a significant reduction of porosity and permeability. Deformation bands usually show displacements of only a few millimeters to centimeters, and similar thickness, and cannot be captured by seismic measurements.

This study analyzed five core samples taken from a well in a hydrocarbon reservoir, the Matzen Field, of the Vienna Basin. The well is located near large normal faults. The samples were selected from depths between 1647.5m and 1656.5m, where deformation bands were identified. The Badenian terrigenous Matzen sandstones contain predominantly quartz, feldspar and dolomite as sub-rounded, detrital grains bearing weak cementation. Normal faults with several tens to hundreds of meters of displacement are well documented from seismic sections, whereas deformation bands in this reservoir have not been studied in detail. These structures may be associated with a significant reduction in porosity, and may thus create barriers to the migration of hydrocarbons and result in a compartmentalization of the reservoir during migration, charging or production.

Deformation bands occur as single bands of up to 4mm width, or as strands of several bands with up to 5cm thickness. Based on grain size analyses of detrital quartz, cataclastic grain size reduction within the bands can be documented. A reduction of porosity within the deformation bands can already be recognized macroscopically and is confirmed by image analysis from back-scattered electron (BSE) images. The porosity is reduced from 20-30% in the host rock to 1-9% in the deformation bands.

In contrast to most published examples of deformation bands in terrigenous sandstones, the reduction of porosity is predominantly caused by precipitation of Fe-dolomite cement within the bands, and only subordinately by cataclasis. The chemical composition of this cement differs from the detrital dolomite grains of the host rock. The dolomite cement shows 10-12wt% FeO content, in contrast to the detrital dolomite grains with less than 2wt% FeO. This observation suggests that the cement is not derived from the detrital grains, but precipitated from a fluid from an external source.

In summary, the evolution of deformation bands in the Matzen reservoir can be characterized as follows: After an initial increase of porosity by dilation, disaggregation and fragmentation of detrital grains, a Fe-rich carbonate fluid crystallized within the bands, thereby reducing the porosity relative to the host sediment. Regarding the origin of the Fe-rich dolomite cement, it is postulated that fluids enriched in Fe and Mg originating from underlying shale layers were precipitated within the bands.

Different degrees of oil staining on either side of the bands demonstrate that these cementation bands act as effective barriers to the migration of hydrocarbons and should be considered in reservoir models.

Zusammenfassung

In porösen Sedimentgesteinen werden Störungszonen häufig von Deformation Bands begleitet. Diese flachen Versatzzonen zeigen vorrangig Kornrotation und in einigen Fällen Kornzerkleinerung. Diese Mechanismen haben oft zur Folge, dass es zu einer signifikanten Porositäts- und Permeabilitätsreduktion kommt. Für gewöhnlich zeigen Deformation Bands einen nur kleinen Versatz im Millimeter bis kleineren Zentimeterbereich, eine ähnliche Dicke und können durch seismische Messungen nicht erfasst werden.

In dieser Studie wurden fünf Bohrkernproben des Kohlenwasserstoffreservoirs im Wiener Becken, dem Matzen Feld, analysiert. Die Bohrung findet sich nahe einer großen Abschiebung und die ausgewählten Gesteinsproben wurden aus einer Tiefe von 1647,5m bis 1656,5m entnommen, wo Deformation Bands erkannt wurden. Die aus dem Badenium stammenden terrigenen Matzen Sandsteine enthalten überwiegend Quarz, Feldspat und Dolomit, in Form angerundeter, detritärer Körner und sind kaum zementiert. Abschiebungen mit mehreren Zehnern bis Hunderten Metern Versatz sind anhand seismischer Untersuchungen gut dokumentiert, allerdings wurden Deformation Bands in diesem Reservoir nicht im Detail untersucht. Diese Strukturen können mit einer signifikanten Porositätsreduktion assoziiert werden und können demzufolge Barrieren für das Migrieren der Kohlenwasserstoffe bilden. Daraus ergeben sie eine Kompartimentierung des Reservoirs während der Migration, Anreicherung oder Produktion.

Deformation Bands treten als einzelne Bänder von bis zu 4mm Breite, oder im Verbund mit einer Dicke von bis zu 5cm auf. Basierend auf Korngrößenanalysen detritärer Quarzkörner kann eine kataklastische Korngrößenreduktion innerhalb der Bänder dokumentiert werden. Eine Porositätsreduktion innerhalb der Deformation Bands ist makroskopisch erkennbar und wird durch Bildanalysen von Back-scattered electron (BSE) Bildern bestätigt. Die Porosität wird vermindert von 20-30% im Muttergestein auf 1-9% in den Deformation Bands.

Im Gegensatz zu häufig publizierten Beispielen von Deformation Bands in terrigenen Sandsteinen wird in diesem Fall die Porositätsreduktion hauptsächlich durch Beteiligung von Fe-Dolomitzementen innerhalb der Bands verursacht und nur untergeordnet durch Kataklasten. Die chemische Zusammensetzung des Zements unterscheidet sich von detritären Dolomitkörnern im Nebengestein. Der Dolomitzement zeigt einen FeO-Gehalt von 10-12wt%, im Gegensatz zu den detritären Dolomitkörnern, die weniger als 2wt% FeO aufweisen. Diese Beobachtung weist

darauf hin, dass der Zement nicht durch die Auflösung und Rekristallisation detritärer Dolomitmörner gebildet wurde, sondern von einem Fluid einer externen Quelle stammt.

Zusammenfassend kann die Bildung der Deformation Bands im Reservoir Matzen folgendermaßen charakterisiert werden: Nach einer anfänglichen Porositätszunahme durch Ausdehnung, Auflockerung und Fragmentierung der detritären Körner, kristallisierte ein Fe-reiches Karbonatfluid innerhalb der Bands aus, wobei es zu einer Porositätsreduktion relativ zum Nebengestein kam. Die Fe und Mg-reichen Fluids stammen wahrscheinlich aus darunter liegenden Tonschichten. Unterschiedliche Ölsättigungen auf beiden Seiten der Bänder demonstrieren, dass diese Zementationsbänder als effektive Barrieren für die Migration von Kohlenwasserstoffen agieren und deshalb in Reservoirmodellen berücksichtigt werden sollten.

Introduction

Deformation bands frequently accompany major faults in porous sedimentary rocks (Aydin, 1978). Several characteristic features of deformation bands allow a distinction from brittle fractures (e.g. slip surfaces or joints; Aydin et al., 2006). Generally, they are tabular zones of distributed strain. Accordingly they are wider but show a smaller offset than striated slip surfaces. Compared to brittle fractures, where cohesion is lost or reduced, deformation bands retain or increase cohesion. Furthermore, a reduction in porosity and permeability is observed within most deformation bands. These attributes may influence fluid flow in groundwater and hydrocarbon reservoirs (Sternlof et al., 2006; Kolyukhin et al., 2010). Commonly, deformation bands occur as single bands with a width up to a few millimeters or as strands of several bands up to a few centimeters or decimeters in total width (Fossen et al., 2007).

Deformation bands can be classified according to their kinematic properties (Aydin et al., 2006), as shear, compaction, or dilation bands; hybrids exist between these end members. Shear bands are frequently accompanied by compaction (i.e. pore space reduction), caused by grain rotation, grain sliding and/or grain fracturing (Eichhubl et al., 2010, and references therein). Early stages of shear bands can include a component of dilation, which has been identified in both theory and in the field (Du Bernard et al., 2002; Bésuelle, 2001; Borja and Aydin, 2004).

Additionally, deformation bands are classified by their deformation mechanism (Fossen et al., 2007), which depends on grain size, shape, sorting, cementation, mineralogy and porosity of the host sediment, and on the stress conditions during the formation of the bands. Disaggregation bands are characterized by sliding and rotation of individual grains, without significant fracturing. Phyllosilicate bands contain 10% to 15% platy minerals within the bands. Cataclastic bands are dominated by grain fracturing. If cementation or dissolution occurs preferentially along deformation bands, they are classified as cementation and solution bands. Cementation bands are not regularly documented in geological literature. Deformation bands characterized by cementation were described by Sample et al. (2006), Parnell et al. (2004) and Parnell (2009).

This study examines deformation bands in Neogene sandstones of the Vienna Basin, a Miocene pull-apart basin in the North East of Austria. Core samples were analyzed from the Matzen field, one of the largest onshore hydrocarbon reservoirs in Central Europe. This area is thus one of the

best studied parts of the Vienna Basin concerning stratigraphical, lithological and structural content. The dominant fault system with conjugated normal faults indicates (late) Miocene NW-SE extension, and is well documented in numerous 2D and 3D seismic datasets (Hinsch et al., 2005). However, deformation bands related to the larger faults have not been investigated so far. This thesis focuses on deformation bands from a depth of ca. 1650m. They originate from a unit underlying the main reservoir, the Matzen sands, which were deposited during a lower Badenian (ca. 15 Ma) marine transgression in the Vienna Basin.

The collected microstructural and chemical data provide insight into the kinematic evolution and timing of the deformation bands, as well as the mineralogical and petrophysical alteration with respect to the surrounding rock. The findings characterize and describe the influence of the deformation bands on the migration of hydrocarbons and on the reservoir quality.

Geological Setting

The Vienna Basin (Figure 1) is part of the Neogene Paratethys basin system (Steininger and Wessely, 2000). It is located in northeast Austria, extending into Slovakia and the Czech Republic, between the Eastern Alps and the Western Carpathians (Royden, 1985; Wessely, 1988). The Miocene, 200 km long and 60 km wide, rhombohedral pull-apart basin was formed along NNE-SSW trending strike-slip faults during lateral extrusions of the Eastern Alps (Ratschbacher et al., 1991; Decker, 1996; Decker and Peresson, 1996, Linzer et al., 2002; Wagreich and Schmid, 2002). The evolution of the Vienna Basin can be divided into two major stages (see also Royden, 1985, 1988; Decker, 1996; Decker et al., 2004):

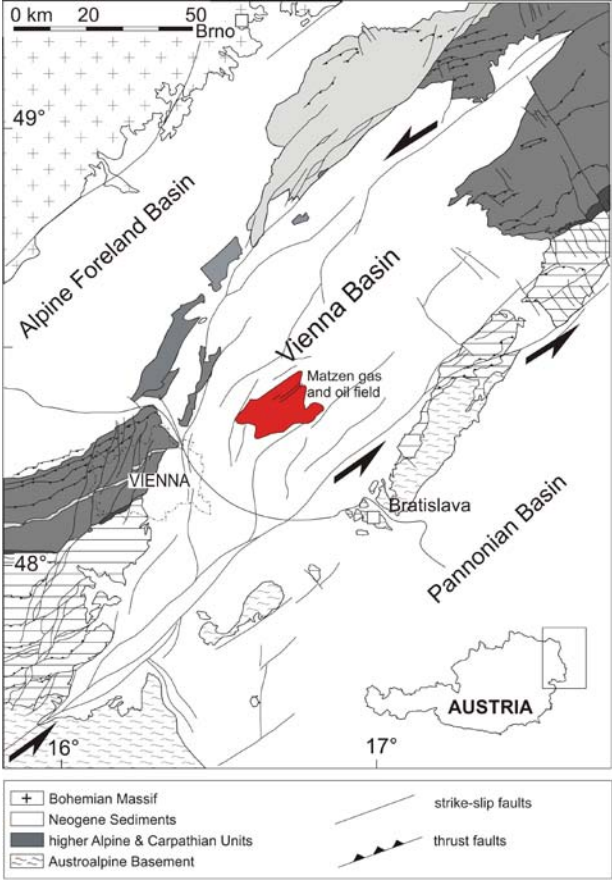


Figure 1: Geographical and geological overview of the Matzen Field in the central Vienna Basin (modified after Brix and Schulz, 1993).

In the Early Miocene (ca. 23-16.4 Ma, Figure 2), the basin was formed as an E-W trending piggy-back basin developing on top of the active NW-directed Alpine thrustbelt (e.g. Decker, 1996; Seifert, 1996; Hamilton et al., 2000). During the Middle and Late Miocene (ca. 16.4-7.1 Ma), thrusting was followed by lateral extrusion of crustal blocks east of the Tauern Window, and the basin evolved into a pull-apart basin bordered by sinistral strike-slip faults (Royden, 1985, 1988; Wessely, 1988). This change can be recognized in the depositional sequence of the Vienna Basin as a major regressive event at the Karpatian/Badenian boundary (Roegl et al., 2002; Wagneich and Schmid, 2002). Rapid subsidence is responsible for an accumulation of ca. 5.5km of sediments in the central part of the Vienna Basin (Hoelzel et al., 2008).

The samples investigated in this study are from the central part of the Vienna Basin, within the Matzen Oil and Gas Field. In this part of the basin, the earliest deposits unconformably overlie the pre-Neogene basement. The sedimentation can be characterized as lacustrine to brackish-littoral in the basal units, (Bockfliess Formation, Roegl et al., 2002), followed by a lacustrine-terrestrial sequence (Gaenserndorf Formation, Kreutzer, 1992) to limnic-fluvial on top (Aderklaa Formation, Weissenbaeck, 1996). More precisely, the analyzed samples belong to the Auersthal beds of the informally named stratigraphic unit 'Untere Sande', which underlies the gas and oil bearing "Tortonian" horizons of Badenian age (Figure 2). The unit 'Untere Sande' comprised of the Bockfliess Beds, Gänserndorf Beds, Aderklaa Beds, followed by the Aderklaa Conglomerates, Auersthal Beds and the Upper Lagenid Zone (Papp et al., 1973).

During the Early Badenian, a fluvial succession (Aderklaa Conglomerates) was deposited in the southern Vienna Basin during a sea-level lowstand. These sediments were transported to the north by a braided river system (Papp and Steininger, 1987). The fluvial development was followed by a marine transgression. The marine ingression came through a seaway connecting the basin with the Mediterranean area to the South. During the Sarmatian (ca. 13-11.5 Ma) the marine environment gradually changed to brackish water conditions. It is characterized by meandering channels and delta deposits and correlates with the final isolation of the Paratethys from the Mediterranean Sea. The Late Miocene (ca. 11.5-7.1 Ma) is characterized by a decrease in salinity, leading to lacustrine and fluvial deposits (Sauer et al., 1992; Roegl and Daxner-Hoek, 1996; Seifert, 1996).

Ma	series	stage	NN-zones	lithostratigraphic units biostratigraphic zones	environment
8	LATE MIOCENE	7.1 PANNONIAN	NN11	Upper Pannonian	decreasing salinity ↑
9			NN10		
10			NN9b	[9.8] Middle Pannonian [10.2]	
11			NN9a/8	Lower Pannonian	
12			NN7	Upper Sarmatian [12.2]	
13	MIDDLE MIOCENE	11.5 SARMATIAN	NN6	Lower Sarmatian	brackish (deltaic)
14			NN5	Bulimina-Rotalia zone [13.8]	marine
15				Spiroplectammina zone [14.4]	
16				Upper Lagenid zone [15.5]	
17				Lower Lagenid zone [16.1]	
18	Aderklaa conglomerate	fluviatile			
17	E. MIOCENE	16.4 KARPATIAN	NN4	Aderklaa Fm.	limnic/ fluviatile
				[17.0] Karp. flysch debris	terrestrial
				[17.2] Gänserndorf Fm.	
17		17.3		Basement	pre-Neogene units

Figure 2: Stratigraphy of the Vienna Basin, after Wagreich and Schmid, 2002.

Matzen Field

The Matzen oil and gas field, located 30 km northeast of Vienna, is one of the largest onshore hydrocarbon reservoirs of Central and Western Europe and the main reservoir of the Vienna Basin (Fuchs and Hamilton, 2006, Figure 1). Since the discovery of the field in 1949, extensive exploration by the OMV was carried out.

The oil and gas is reservoided in shallow-marine to fluvial clastic sediments of Middle and Late Miocene age (Badenian, Sarmatian and Pannonian).

To date, about 1500 wells have been drilled, which produced 516 million bbl oil and 1.1 tcf gas, which represent about 90% of the established initial reserves of the entire Matzen field (Fuchs and Hamilton, 2006). The acquisition of high-resolution 3D seismic data in the 1990's promoted a series of new sedimentological and structural studies (e.g., Fuchs and Hamilton, 2006; Hinsch et al., 2005; Strauss et al., 2006; Hoelzel et al., 2008). Detailed mapping of horizon and fault surfaces revealed a complex system of fault-bounded hosts and grabens (Figure 3).

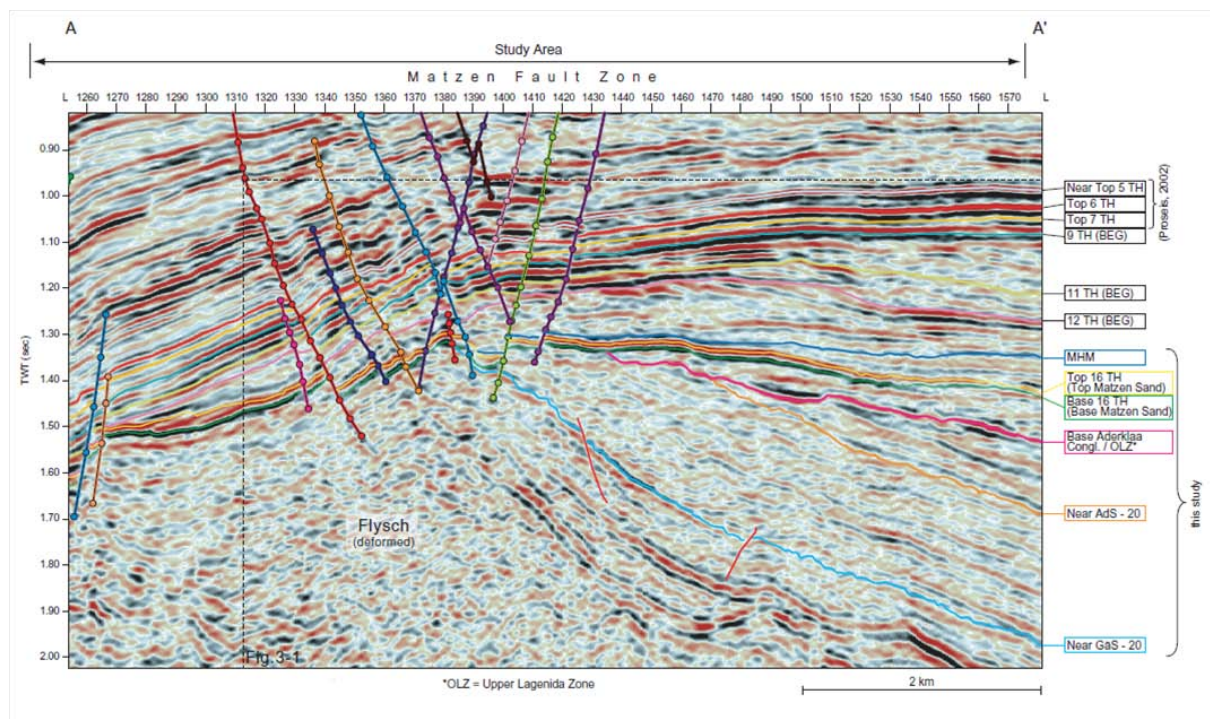


Figure 3: Seismic image of the Matzen Fault, OMV Report, 2003

Structurally, the Matzen field can be divided into four different zones, (i) the Matzen anticline, an elongated, NE-SW trending anticline, which is located in the central part of the field, (ii) the Matzen fault system, a pull-apart graben in the north bounded by sinistral strike-slip faults, (iii) the Bockfliess fault system in the west and (iv) the Markgrafneusiedl normal fault zone in the south (Schroeckenfuchs, 1975; Fuchs and Hamilton, 2006).

Samples and Methods

Samples

The samples investigated in this study derive from cores taken from a depth of 1647.5 m to 1656.5 m (Figure 4) in well Matzen 220, which is located in the center of the Matzen field. The sandstone samples, with a diameter of 12 cm, are from the top of the informally named 'Untere Sande' unit of Badenian age. They directly underlie the most prominent reservoir unit in the Vienna Basin, the 16 TH horizon. The sandstones are weakly to moderate cemented-litharenites with a grain size of up to 0.3mm (middle sand).

Deformation bands can be recognized in several sections of the core. The thickness of individual bands ranges from 2 to 4 mm; in some cores anastomosing strands of deformation band reach a combined thickness of up to 5 cm (Figure 5). Due to the fact that the cores are broken up into cm-dm long, discontinuous sections, the length of the bands cannot be determined (Figure 4). Some of the samples show extensive oil staining (e.g. MA220-1656.5, Figure 4), which is partially restricted to one side of the bands.



Figure 4: The five core samples from Matzen 220 analyzed in this study. Note the oil staining in the lower right image.



Figure 5: Core sample with deformation bands, 1651 m.

Methods

To determine the mineralogical composition and microstructural features of the deformation bands and the host material, the following analytical devices at the Department of Geodynamics and Sedimentology, and the Department of Lithospheric Research at the University of Vienna were used.

Optical Microscopy

Sandstone samples were investigated with optical microscope Leica DM 4500P equipped with a digital color camera, Leica DFD295 with 3 megapixels. The images were processed with the Leica[®] Assistance Software (LAS) V3.2.0. The most commonly used objective lenses were 5.0x and 10.0x. The studied thin-section samples have a thickness of 30 μm . Thin-sections were stained with Alizarin Red S and K-ferricyanide for carbonate mineral determination. Sandstone modal composition was determined by counting 200 points per thin section.

X-Ray Diffraction (XRD)

X-ray diffraction provides qualitative and semi-quantitative information about the bulk mineralogy of the samples. The analysis was made with a Panalytical X'Pert PRO diffractometer (CuK α radiation, 40 kV, 40 mA, step size 0.0167, 5 s per step). Five sample pairs (deformation band and host rock of each core sample) were powdered to a grain size of <2 μm .

Scanning Electron Microscopy (SEM)

The scanning electron microscope, FEI INSPECT S50, was used to study the morphology and the surface of two split samples. The backscatter electron detector (BSE) and energy dispersive x-ray analysis (EDX) were used to get high-resolution images and to characterize the chemical composition of the samples in thin sections. A high energy electron beam, operating with up to 30 kV supports the device. Element maps were taken with a focus on elements Si, Fe, Mg, Ca

and K. The images were analyzed with the program ImageJ to determine mineralogical composition, porosity and grain size distribution.

Thin-sections were coated with carbon to avoid charging and achieve conductivity of the electron beam. The sandstone split samples used in the SEM had a size of 0.5 cm x 1 cm x 0.5 cm. They were coated with a thin gold layer for the same reasons as the BSE samples.

Electron Microprobe Analysis

Quantitative analysis of the chemical composition of detrital dolomite grains and dolomite cement was performed with a CAMECA SX100 electron microprobe. The beam current was set at 20 nA and the voltage at 15 kV. To avoid charging and to achieve conductivity the thin section samples were coated with a thin carbon layer. Quantitative spot analyses for Fe, Ca and Mg content were performed using the wavelength-dispersive (WDX) spectrometer.

Cathodoluminescence (CL)

A cathodoluminescence microscope, Lumic HC5-LM, was used to identify zoning or fracturing of cements and detrital grains. The thin-sections of 25 μm thickness were coated with carbon for better conductivity. The images were taken with an acceleration voltage set at 14 kV and a beam current of 5-7 mA.

Carbon and Oxygen Stable Isotope Analyses

Samples for carbon and oxygen stable isotope analyses were taken with a handheld micro-drill. Both deformation bands and host rock were analyzed three times each. Sample powders were reacted with 100% phosphoric acid at 70 °C with a Thermo-Finnigan Kiel II automated reaction system. The evolved CO₂ gas was measured with a Thermo-Finnigan Delta Plus isotope-ratio mass spectrometer at the Institute of Earth Sciences at the University of Graz. The $\delta^{13}\text{C}$ and $\delta^{18}\text{O}$ values are corrected according to the NBS19 standard and reported in per mill (‰) relative to the

V-PDB (Vienna-PeeDee Belemnite) Standard. Measurements of NBS-19 and an internal laboratory standard indicate a standard deviation of 0.01‰ for $\delta^{13}\text{C}$ and $\delta^{18}\text{O}$.

Results

In order to constrain the petrophysical properties and kinematic evolution of the deformation bands, we analyzed lithological, diagenetic and microstructural features of the sampled material. The deformation bands can already macroscopically be distinguished from the host rock as dark anastomosing bands of lower porosity (Figure 5).

The polished thin-sections for analysis in the scanning electron microscope and electron microprobe were scanned for a better orientation and overview during analyses. Deformation bands are easily identified as dark gray, anastomosing bands (Figure 6).



Figure 6: Thin-section scan of the sample 1647.5m. Deformation bands are clearly visible as dark, anastomosing bands of 3-10 mm thickness.

Under the optical microscope, the cause for this porosity reduction can be identified as micritic carbonate cement. The thin-section image of 1651m shows the boundary of a deformation band to the host rock (Figure 7). The detrital grains quartz, feldspar and dolomite are weakly cemented by carbonate in the host, and completely cemented inside the deformation band.

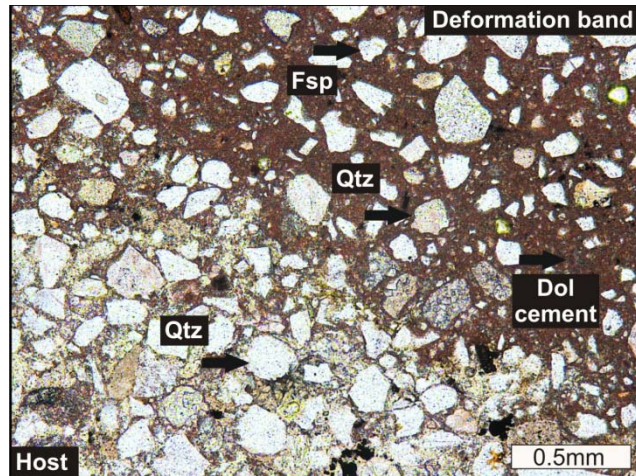


Figure 7: Thin section image of sample 1651m in plane polarized light (PPL), showing the boundary of a deformation band (upper right) to the host rock. The detrital grains of quartz (Qtz), feldspar (Fsp) and dolomite (Dol) are weakly cemented by carbonate in the host, and completely surrounded by cement inside the deformation band.

Lithology

The investigated sandstones can be classified as litharenites (after Folk, 1968, Figure 8), determined by point-counting of 200 minerals in each of the five analyzed thin-sections. The detrital grains show a low sphericity, are angular to subrounded and are well sorted with a grain size between 0.05mm and 0.4mm.

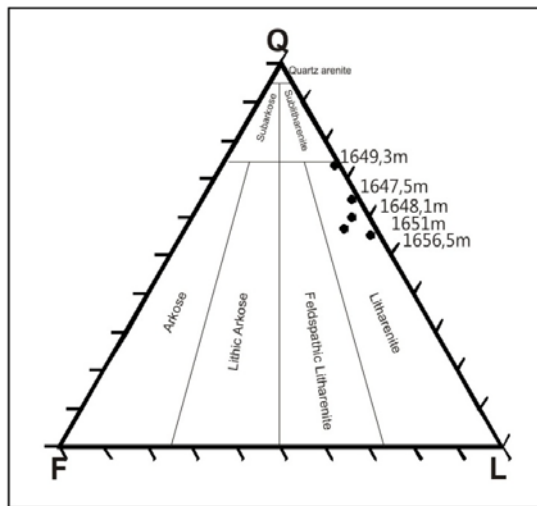


Figure 8: All samples can be classified as litharenite in diagram plotting quartz (Q), feldspar (F) and lithic grains (L) (after Folk, 1968).

In all the samples analyzed in this study, the mineralogical composition is identical in the host rock and the deformation bands. The sandstone samples are dominated by quartz, detrital dolomite grains, feldspar, and pyrite; the pore space is partly cemented by dolomite in the host rock. In contrast, the relative content of dolomite is increased by a factor of 2-3 in the deformation bands, whereas the amount of pore space is decreased from 18.4-31.5% to 1.2-9.1 % in the deformation bands (Figure 9).

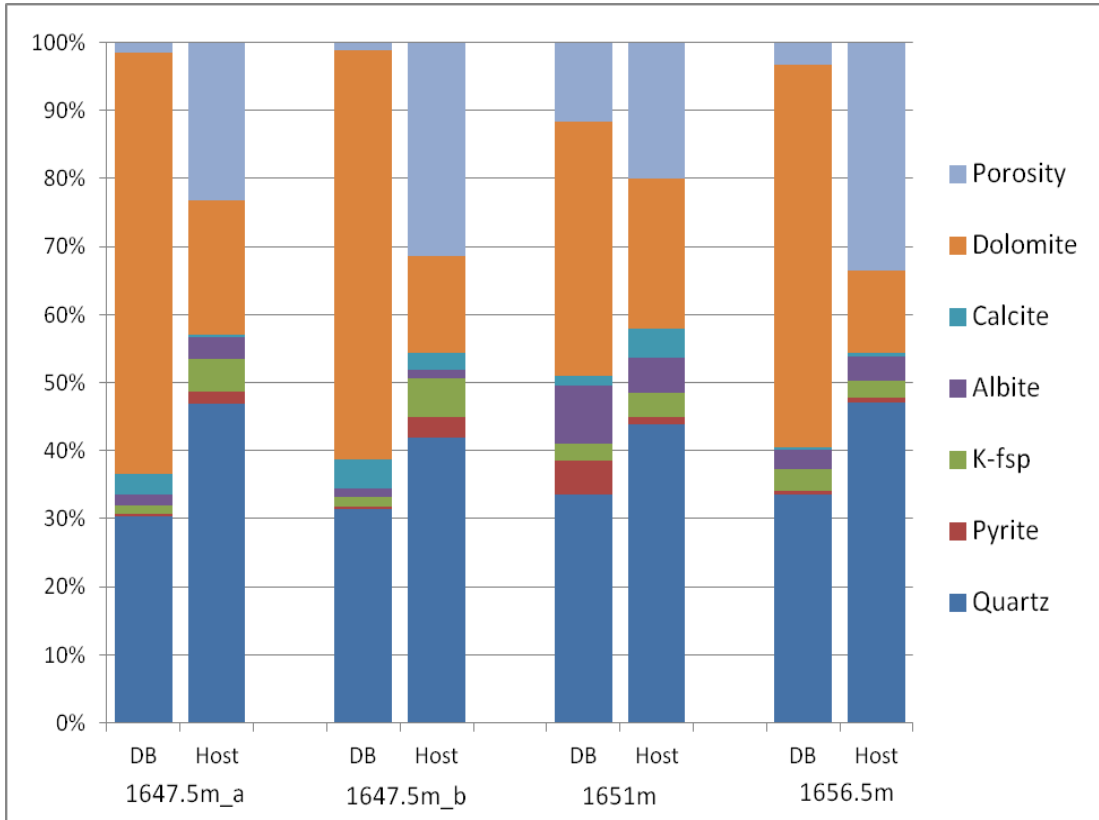


Figure 9: Mineralogical composition of the sandstone samples from various depths (DB=deformation band, Host=host rock). A decrease in porosity correlates with an increase in dolomite cement in the deformation bands relative to the host rock.

Qualitative information of the mineralogical composition from X-ray diffraction patterns indicates no significant difference between the deformation band and host rock. The peak intensities of the diffraction pattern suggest that the percentages of some minerals of the deformation bands vary relative to the host rock, e.g. for dolomite with a higher peak (Figure 10). Chlorite, muscovite, kaolinite, ankerite and feldspar appear with nearly the same concentration.

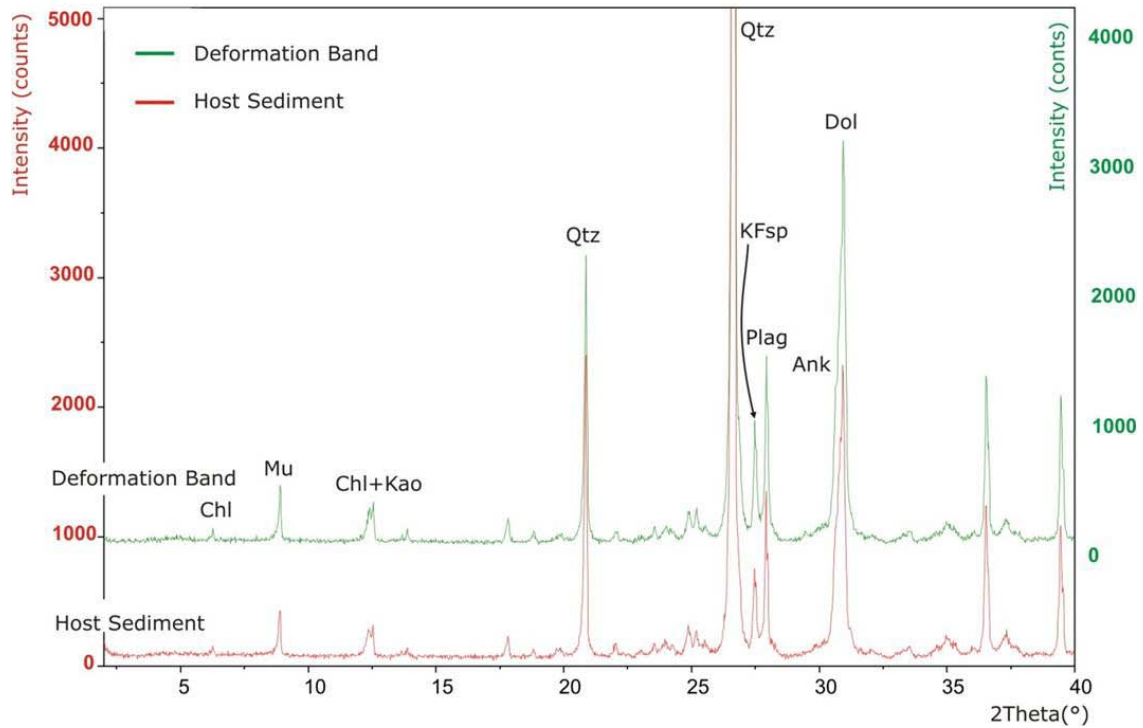


Figure 10: X-ray diffraction pattern, mineralogical composition of deformation band and the host sediment

(Chl=chlorite, Mu=muscovite, Kao=kaolinite, Qtz=quartz, KFs=K-feldspar, Plag=plagioclase, Ank=ankerite,

Dol=dolomite, 1648.1m)

Diagenetic processes

The dolomite cement and detrital dolomite grains of sample 1649.5 m show bright red luminescence (Marshall,1988), in contrast to the non-luminescent quartz and weakly luminescent K-feldspar (blue) or plagioclase (green)(Figure 11). The boundary between host rock (left side of the image) and deformation band (right side) is clearly evident, due to the higher content of luminescent dolomite cement in the deformation band. Dolomite cement rims grow often on detrital dolomite and quartz grains both within deformation bands and in the host rock (Figure 12).

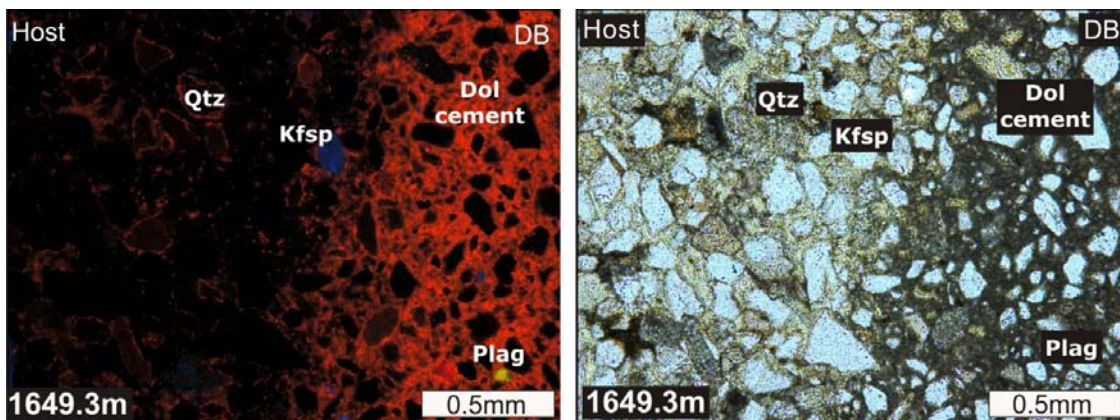


Figure 11: Cathodoluminescence (left) and transmitted light (right) images of the transition from deformation band (DB) to host rock (Host), 1649.3m; red luminescence indicates dolomite cement and detrital dolomite grains (Dol=dolomite, Qtz=quartz, Kfsp=K-feldspar, Plag=plagioclase).

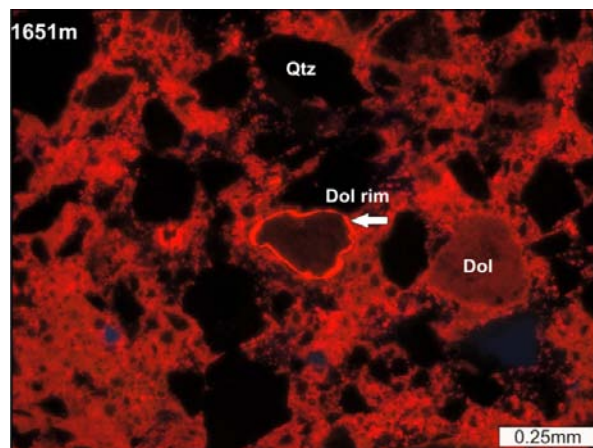


Figure 12: Cathodoluminescence image showing a detrital dolomite grain with dolomite cement rim of bright red luminescence within the deformation band, 1651m.

Dolomite cement and authigenic kaolinite on a quartz grain can be observed on an untreated split sample (Figure 13 A) in the scanning electron microscope. The dolomite cement grains have a characteristic euhedral orthorhombic shape and are between 2 and 5 μm in size. Kaolinite shows vermiform face-to-face stacks of pseudo-hexagonal plates, of ca. 10 μm diameter. Another split sample was treated with hydrochloric acid to dissolve the carbonate cements. The surface of quartz grains is etched by idiomorphic dolomite grains, leaving rhombic dissolution pits (Figure 13 B).

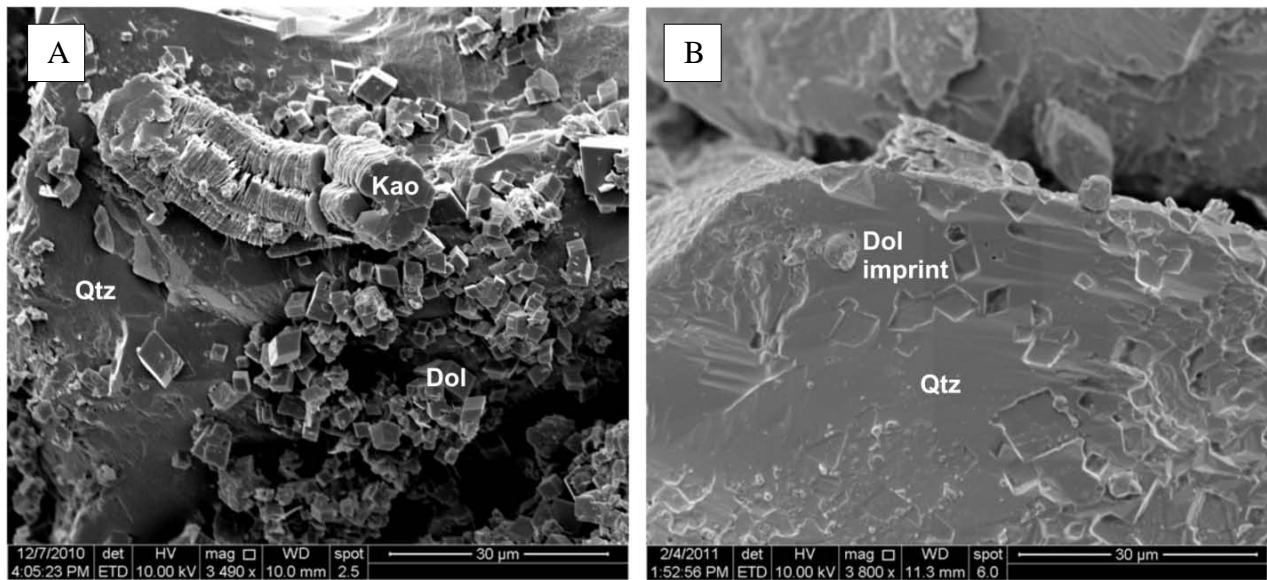


Figure 13: Split sample showing kaolinite (Kao) and dolomite cement (Dol) on quartz grain (Qtz), 1647.5m (A); split sample treated with hydrochloric acid showing quartz grains (Qtz) with imprints of dissolved dolomite grains (Dol imprint), 1647.5m (B).

Quantitative measurements of the chemical composition of both detrital dolomite grains as well as the dolomite cement were performed with the electron microprobe (Figure 14 A). The dolomite cement shows a significant higher iron concentration (10-12 wt% FeO) compared to the detrital dolomite grains (0-2 wt% FeO). Some detrital dolomite grains reveal chemically zoned growth rims of dolomite cement, with an increasing Fe-content indicated by higher intensities in the BSE image (Figure 14 B).

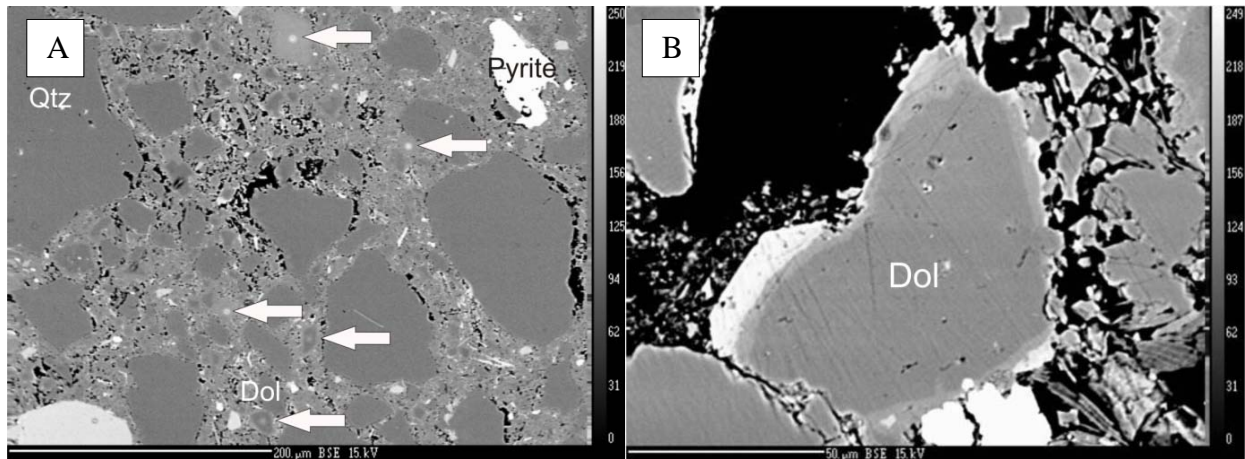


Figure 14: BSE image of a deformation band; white arrows showing the points, where the Fe-concentrations was measured, 1651m (A); BSE image showing detrital dolomite grain (Dol) with Fe-rich rims, 1651m (B).

The stable carbon and oxygen isotopes of the host rock and the deformation band were measured to determine the origin of the carbonate cement. A general trend can be observed for most of the measured host rock - deformation band pairs, shifting the corresponding deformation band isotopic composition towards more positive $\delta^{18}\text{O}$ and more negative $\delta^{13}\text{C}$ values than the host rock (Figure 15). The $\delta^{13}\text{C}/\delta^{18}\text{O}$ values of the host rock fall between -2 and -0.5‰ for $\delta^{18}\text{O}$ and 0 and +3.5‰ for $\delta^{13}\text{C}$. The deformation bands show a distribution between -0.3 and +0.9‰ for $\delta^{18}\text{O}$ and -1.5 and +0.6‰ for $\delta^{13}\text{C}$. Only sample 1648.1 m does not follow this general trend.

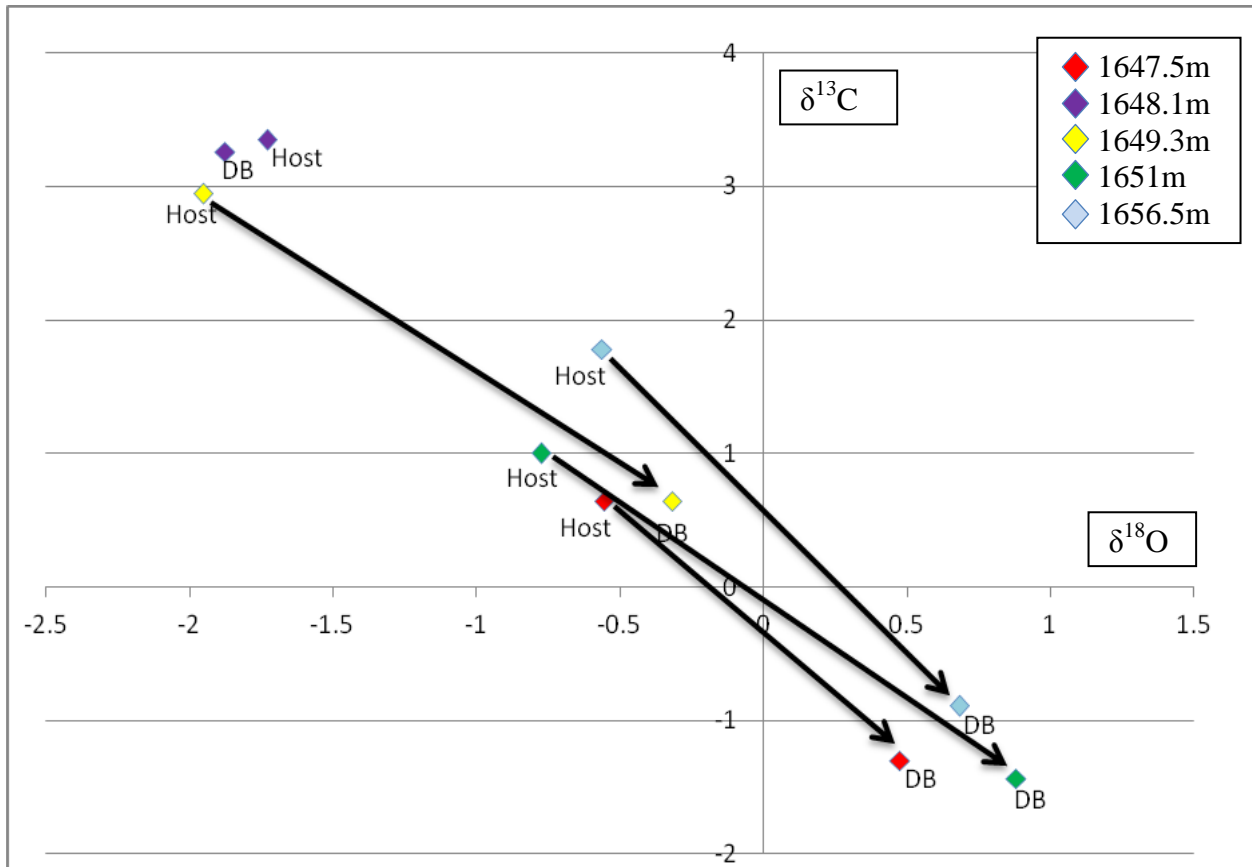


Figure 15: Carbon and Oxygen Stable Isotope Analysis (Host= Host rock, DB= Deformation Band); a trend can be observed for samples 1647.5m, 1649.3m, 1651m and 1656.5m, all showing a similar shift towards positive $\delta^{18}\text{O}$ and negative $\delta^{13}\text{C}$ values.

Microstructures

In contrast to typical cataclastic deformation bands described in sandstones (e.g., Aydin, 1978), only few fractured grains can be observed in the studied samples. Some few broken grains, primarily quartz grains, can be recognized within the deformation bands embedded in pyrite cement (Figure 16 A), at the border to the host rock (Figure 16 B), and in the split sample (Figure 16 C). The most significant difference between the deformation band and the host rock is the presence of up to ca. 40% of dolomite cement within the deformation bands (see Figure 11). At the rim and across some deformation bands, fractures cutting across both detrital grains and dolomite cement are observed (Figure 16 D), suggesting a formation of these fractures after the cementation.

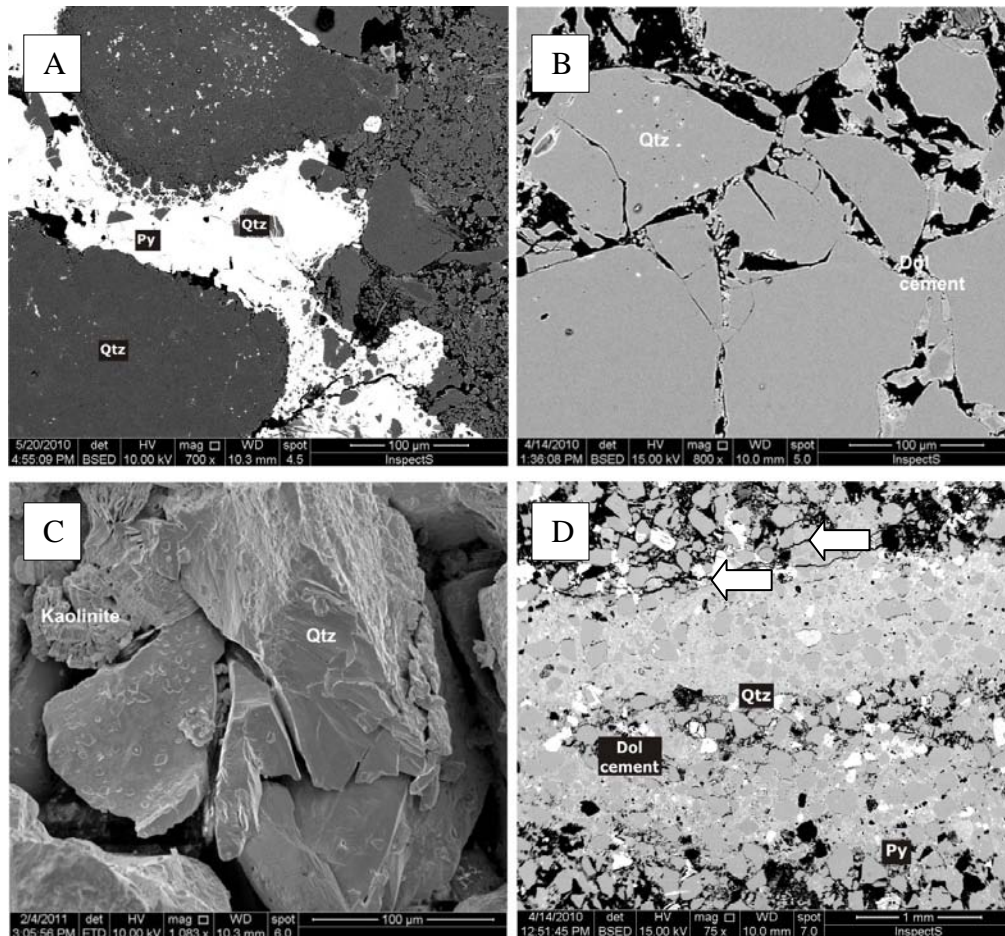


Figure 16: Broken quartz grain embedded in pyrite cement, BSE image, 1649.3m (A); BSE image and split sample showing broken quartz grains in detail (1647.5m, B, C), sandstone sample comprise fractures along host rock and deformation band boundary (1647.5m, white arrows, D).

The grain size distribution within deformation bands and the host rock was analyzed, from BSE images and element maps, in order to identify potential grain size reduction within the deformation bands prior to cementation. For a reliable statistical analysis, the dominating mineral phase was used, i.e. quartz, for the grain size analyses. One of the investigated areas, at the margin of a deformation band (Figure 17 A), shows quartz grains as the most intense phase in a Si-element map (Figure 17 B). From this image, the quartz grains were extracted (Figure 18) and the area of each grain was computed using ImageJ. As already evident in the binary image, the grain size is reduced within the deformation band (Figure 19), resulting both in a decrease in size of the quartz grains (ca. 150-250 μm in diameter), as well as in an increase in the amount of small grains ($< 25 \mu\text{m}$ diameter).

Additionally, the distribution of dolomite cement, detrital dolomite grains and porosity can be analyzed in the element maps. The high intergranular porosity in the host rock (ca. 20%) is reduced to ca. 2-5% in the deformation band (Figure 17 A). The magnesium (Figure 17 C) and calcium (Figure 17 D) element maps highlight the distribution of detrital dolomite grains and dolomite cement. The dolomite cement essentially covers the entire inter-granular space within the deformation band; but only few pores and grains within the host rock are cemented by a chemically identical dolomite (compare Figure 17A to C and D). Detrital dolomite grains can be observed both in host rock and deformation band, as more compact grains with high intensities in the element maps.

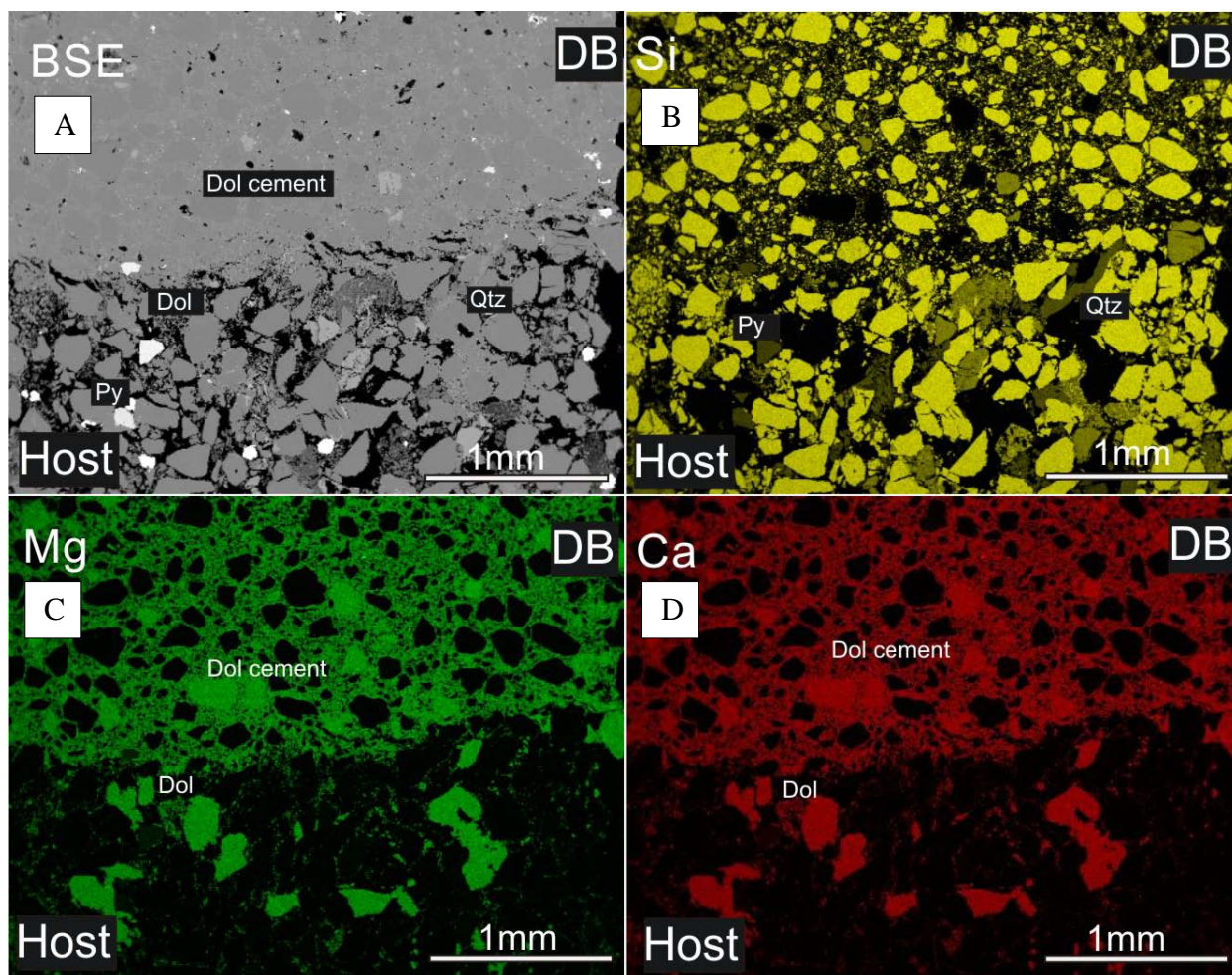


Figure 17: BSE image of sample 1647.5m showing the deformation band on top and the host rock at the bottom (A); element map of Si showing feldspar, mica (gray-yellow) and quartz grains (light yellow, B); the Mg and Ca images display the dolomite grains and cement within the deformation bands and detrital dolomite grains both host rock and deformation band (C, D).

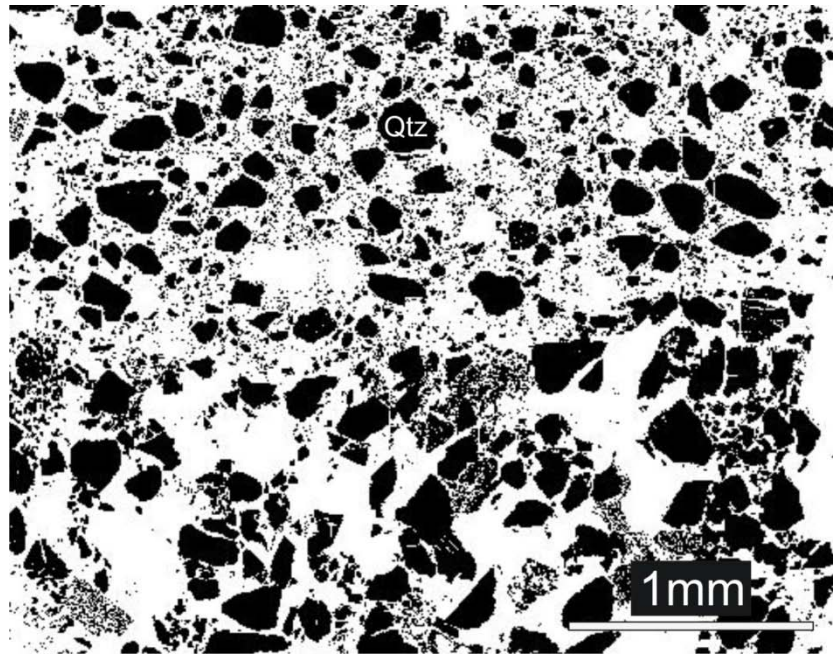


Figure 18: B/W image of host rock and deformation band (1647.5m), which was used to measure grain sizes of quartz grains.

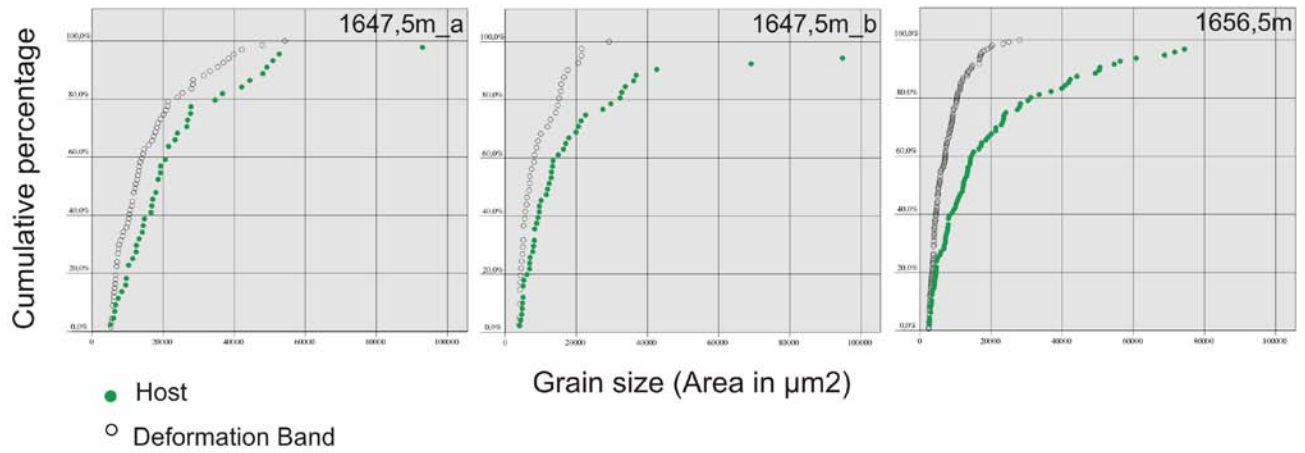


Figure 19: Grain size distributions of quartz grains in deformation band and host rock (1647.5m_a, 1647.5m_b, 1656.5m) display a significant difference. Quartz grains within the deformation band show a smaller grain size compared to the host rock.

Discussion

Combining the mineralogical and microstructural data collected in this study, it is possible to reconstruct the evolution of deformation bands in well core samples from a reservoir of the Matzen oil and gas field in the central Vienna Basin.

Macroscopically it is evident that the main difference between deformation bands and host rock is the porosity. Deformation bands show a more compact texture than the surrounding sandstone (Figure 6). By point-counting and the use of image processing programs the porosity of the deformation bands and the host rock was calculated. The bands show a drastic decrease in porosity with 9% at the maximum, in contrast to the surrounding rock with up to 31.5% porosity. The reason for the decrease in porosity is the precipitation of Fe-rich dolomite within the deformation bands. In summary, the porosity and dolomite content comprise a much larger volume within the deformation bands (48-62%; see Figure 9) than in the host rock (42-46%). This in fact indicates that prior to the precipitation of the dolomite, the porosity within the deformation increased relative to the host rock. Thus, the observed deformation bands can be classified as dilation bands (Du Bernard et al., 2002). These type of bands typically occur in poorly consolidated sandstone at low overburden pressure.

Measured Fe concentrations both in detrital dolomite grains as well as the dolomite cement suggest a different origin of the dolomite cement (10-12 wt% Fe) compared to the detrital dolomite grains (0-2 wt % Fe).

Carbon and oxygen isotope analysis was made in an attempt to identify the origin of the dolomite cement. The measured $\delta^{13}\text{C}$ and $\delta^{18}\text{O}$ ratios indicate a non-meteoric source of the dolomite cement, since all samples display a consistent shift towards lower $\delta^{13}\text{C}$ and higher $\delta^{18}\text{O}$ values with respect to the detrital dolomite (Figure 15, Hoefs, 1973). Thus, the source of the Fe-rich dolomite cement may be hydrothermal fluids associated with normal faults within the Vienna Basin. Alternatively or additionally, the diagenesis of clay minerals in the underlying shales may have released Mg and Fe, contributing to the formation of the Fe-rich dolomite (Boles, 1978; McHargue and Price, 1982; Gawthorpe, 1987; Land et al., 1987; Macaulay et al., 1993; de Souza et al., 1995).

In conclusion, several different stages of deformation band formations are captured within the analyzed samples. An initial dilation associated with some fracturing of grains under low burial

conditions resulted in an increase in porosity (Figure 20 B). Subsequently, the precipitation of Fe-rich dolomite fluid decreased the porosity dramatically within the deformation bands (Figure 20 C and D). In this later stage, the bands can thus be classified as cementation bands (Fossen et al., 2007). Some minor fracturing, parallel and perpendicular, to the deformation bands indicates that the cemented bands are as a result stronger than the surrounding, weakly cemented sandstone. This modification of the petrophysical properties, from porosity increase to porosity decrease and a corresponding variation of the permeability certainly has a major influence on the migration of hydrocarbons in the reservoir (Micarelli et al., 2006; Shipton and Cowie, 2001). This assumption is supported by the observation that oil-bearing samples show a different degree of oil saturation on each side of the deformation bands.

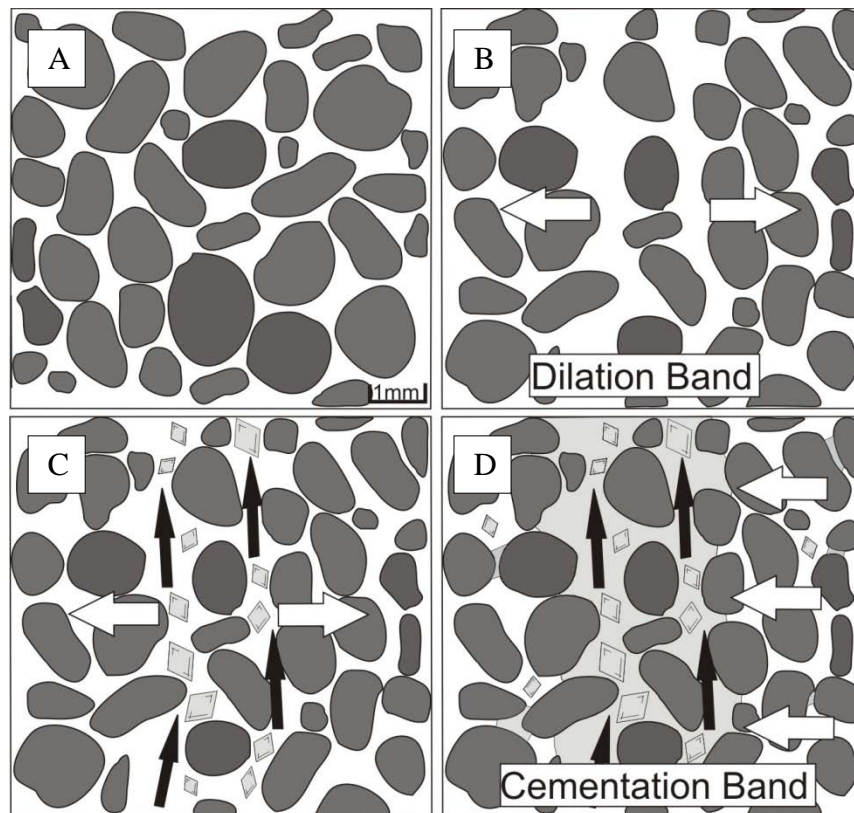


Figure 20: Development of the cementation band. A) initial undeformed sand. B) increase in porosity by extension, forming a dilation band. C) precipitation of an Fe-rich fluid and decreases the porosity, D) forming a cementation band.

Conclusions

Sandstone samples were taken from a well core in the Matzen hydrocarbon reservoir, central Vienna Basin, Austria. The litharenites are mainly composed of quartz, feldspar and detrital dolomite, with angular to subrounded, well sorted grains of low sphericity, cemented by a Fe-rich dolomite. The samples contain numerous deformation bands, which can macroscopically be identified as 1-4 mm broad, mostly anastomosing zones of low porosity.

The comparison of X-ray diffraction patterns of host rock and deformation bands suggest a difference in concentration, especially of dolomite, but not in mineralogical composition. Single point analyses with the electron microprobe demonstrate further differences. The FeO content of the detrital dolomite grains adds up to 2 wt %, in contrast to the dolomite cement with a content of 10-12 wt % FeO. This suggests a clear difference in the origin of the dolomite.

The porosity of deformation band and host rock was calculated by an image-processing program and point-counting. The bands show a drastic decrease in porosity with 9% at the maximum, in contrast to the surrounding rock with up to 31.5% porosity. The reason for the decrease in porosity is the preferred precipitation of Fe-rich dolomite cement within the deformation bands.

A grain size reduction of quartz grains can be observed due to dolomite cementation and cataclasis.

Carbon and oxygen stable isotope analysis indicates that the dolomite cement does not originate from a meteoric source, as the detrital dolomite grains of the host rock, but presumably from hydrothermal fluids (with more negative $\delta^{18}\text{O}$ and $\delta^{13}\text{C}$ values).

As a conceptual model for the development of these deformation bands, a proposition that an initial phase of dilation and shear localization under low burial conditions, associated with some minor cataclastic fracturing of grains, resulted first in an increase of porosity can be made. Subsequently, the high porosity band served as a high permeability pipeline during cementation of the rock by a Fe-rich dolomite. Preferred precipitation of this Fe-dolomite within the band resulted in a reduction of porosity down to 1.2%. Accordingly, the deformation bands can therefore be classified as cementation bands (after Fossen, 2007).

References

- Aydin, A., 1978, Small faults formed as deformation bands in sandstone: *Pure and Applied Geophysics*, v.116, p. 913-930.
- Aydin, A., R. I. Borja and P. Eichhubl, 2006, Geological and mathematical framework for failure modes in granular rock: *Journal of Structural Geology*, v.28, p. 83-98.
- Bésulle, P., 2001, Compacting and dilating shear bands in porous sandstones: *Journal of Structural Geology*, v.106, p. 13,435-13,442.
- Boles, J.R., 1978, Active ankerite cementation in the subsurface Eocene of Southwest Texas: *Contrib. Mineral. Petrol.*, v. 68, p. 13-22.
- Borja, R. I. and A. Aydin, 2004, Computational modeling of Deformation Bands in granular media. I. Geological and mathematical framework: *Computer methods in applied mechanics and engineering*, v.193, p. 2667-2698.
- Brix, F. and O. Schulz, 1993, *Erdöl und Erdgas in Österreich*, 2nd edn. Naturhistorisches Museum, Vienna.
- Decker, K., 1996, Miocene tectonics at the Alpine-Carpathian junction and the evolution of the Vienna basin: *Mitt. Ges. Geol. Bergbaustud. Österr.* v. 41, p. 33-44.
- Decker, K. and H. Peresson, 1996, Tertiary kinematics in the Alpine-Carpathian-Pannonian system: links between thrusting, transformation faulting and crustal extension. In: Wessely, G. and W. Liebl, (Eds.): *Oil and gas in Alpidic Thrustbelts and Basins of the Central and Eastern Europe*: EAGE, Spec. Publ. v. 5, p. 69-77.
- Decker, K., H. Peresson, and R. Hinsch, 2004, Active tectonics and Quaternary basin formation along the Vienna Basin Transform fault: *Quaternary Science Review* v. 24, p. 307-322.
- De Souza, R.S., L.F. De Ros and S. Morad, 1995, Dolomite diagenesis and porosity preservation in lithic reservoirs, Carmopolis Member, Sergipe-Alagoas Basin, northeastern Brazil: *Bull. Am. Ass. Petrol. Geol.*, v.79, p.725-748.
- Du Bernard, X., P. Eichhubl and A. Aydin, 2002, Dilation Bands: A new form of localised failure in granular media: *Geophysical Research Letters*, v. 29, issue: 24, p. 2176.
- Eichhubl, P., J.N. Hooker and S.E. Laubach, 2010, Pure and Shear – Enhanced Compaction Bands in Aztec Sandstone: *Journal of Structural Geology*, v. 32, no. 12, p. 1873-1886.

- Folk, R.L., 1968, *Petrology of Sedimentary Rocks*: Hemphills, Austin, Texas, p.170.
- Fuchs, R. and W. Hamilton, 2006, New depositional architecture for an old giant: The Matzen Field, Austria. In: Golonka, J., & Picha, F.J., (Eds.): *The Carpathians and their foreland: Geology and hydrocarbon resources*: AAPG Memoir v. 84, p. 205-219.
- Fossen, H., R. Schultz, Z. K. Shipton and K. Mair, 2007, Deformation bands in a sandstone – a review. *Journal of the Geological Society*, v. 164, p. 755-769.
- Gawthorpe, R.L., 1987, Burial dolomitization and porosity development in a mixed carbonate-clastic sequence: an example from the Bowland Basin, northern England: *Sedimentology*, v. 34, p. 533-558.
- Hamilton, W., L. Wagner, and G. Wessely, 2000: Oil and Gas in Austria. *Mitt. Oesterr. Geol. Ges.*, v. 92, p. 235-262.
- Hinsch, R., K. Decker and H. Peresson, 2005, 3-D seismic interpretation and structural modeling in the Vienna Basin: implications for miocene to recent kinematics: *Austrian Journal of Earth Sciences*, v. 97, p. 38-50.
- Hoefs, J., 1973, *Stable Isotopes Geochemistry*: Springer Verlag, p. 19-32.
- Hoelzel, M., M. Wagneich, R. Faber and P. Strauss, 2008, Regional subsidence analysis in the Vienna Basin (Austria): *Austrian Journal of Earth Sciences* v. 101, p. 88-98.
- Kolyukhin, D., S. Schueller, M. S. Espedal and H. Fossen, 2010, Deformation Band populations in fault damage zone – impact on fluid flow: *Computational Geosciences*, v. 14, p. 231-248.
- Kreutzer, N., 1992, Matzen field-Austria, Vienna Basin: AAPG, *Treatise-Atlas, Struct. Traps* 7, p. 57-93.
- Land, S.L., K.L. Milliken and E.F. McBride, 1987, Diagenetic evolution of Cenozoic sandstones, Gulf of Mexico Sedimentary Basin: *Sediment .Geol.*, v. 50, p. 195-225.
- Linzer, H.G., K. Decker, H. Peresson, R. Dell'mour and W. Frisch, 2002, Balancing lateral orogenic float of the Eastern Alps: *Tectonophysics* v. 354, p. 211-237.
- Macaulay, C.L., R.S. Haszeldine and A.E. Fallick, 1993, Distribution, chemistry, isotopic composition and origin of diagenetic carbonates: Magnus Sandstone, North Sea: *J. sediment. Petrol.*, v. 63, p. 33-43.
- Marshall, D.J., 1988, *Cathodoluminescence of Geological Materials*. Boston: Unwin Hyman. 146pp.

- McHarguem T.R. and R.C. Price, 1982, Dolomite from clay in argillaceous marine associated carbonates: *J. sediment. Petrol.*, v. 52, p. 873-886.
- Micarelli, L., A. Benedicto and C.A.J. Wibberley, 2006, Structural evolution and permeability of normal fault zones in highly porous carbonate rocks: *Journal of Structural Geology*, v. 28, p. 1214-1227.
- Papp, A., W. Krobot and W. Hladecek, 1973, Zur Gliederung des Neogens im Zentralen Wiener Becken: *Mitt. Ges. Geol. Bergbaustud. Österr.* v. 22, p. 191-199.
- Papp, A. and F. Steininger, 1987, Holostratotypus: Baden-Sooss. In: Papp, A., Cicha, I., Senes J. and Steininger, F. (Eds.): M4 Badenian (Moravien, Wielicien, Kosovien). *Chronostratigraphy und Neurostratotypen, Miozaen der Zentralen Paratethys 6*, VEDA, Bratislava, p. 138-145.
- Parnell, J., G.R. Watt, D. Middleton, J. Kelly and M. Baron, 2004, Deformation Band control on hydrocarbon migration: *Journal of Sedimentary Research*, v. 74, p. 552-560.
- Parnell, J., 2010, Potential of palaeofluid analysis for understanding oil charge history: *Geofluids*, v.10, p.73-82.
- Proseis AG (Zurich), 2003, Matzen Field (Vienna Basin, Austria), Geophysical, Stratigraphic and Petrophysical Evaluation of the 16th Tortonian Oil Reservoir, - Report for OMV AG, Vienna. P. 90.
- Ratschbacher, L., W. Frisch and H. G. Linzer, 1991, Lateral extrusion in the eastern Alps, part II: Structural analysis: *Tectonics* v. 10, p. 257-271.
- Roegl, F. and Daxner-Hoeck, 1996, Late Miocene Paratethys correlations. In: Bernor, R.L., Fahlbusch, V. and Mittmann, H.W., (Eds.): *The evolution of Western Eurasian Neogene mammal faunas*, Columbia Press, New York, v. 3, 47-55.
- Roegl, F., S. Spezzaferri and S. Coric, 2002, Micropaleontology and biostratigraphy of the Karpatian-Badenian transition (Early-Middle Miocene boundary) in Austria (Central Paratethys). *Cour. Forschungsinst. Senckenberg* 237, p. 47-67.
- Royden, L.H., 1985, The Vienna basin: a thin-skinned pull-apart basin. In: Biddle K.T. and Christie-Blick N. (Eds.): *Strike-slip deformation, basin formation and sedimentation*. *SEPM Spec. Publ.* 37, p. 319-339.
- Royden, L.H., 1988, Late Cenozoic tectonics of the Pannonian basin system. In: Royden L. and Horvath F. (Eds.): *The Pannonian basin. A study in basin evolution*: AAPG v. 45, p. 27-48.

- Sample, J.C., S. Woods, E. Bender and M. Loveall, 2006, Relationship between deformation bands and petroleum migration in an exhumed reservoir rock, Los Angeles Basin, California, USA: *Geofluids*, v. 6, p. 105-112.
- Sauer, R., P. Seifert and G. Wessely, 1992, Guidebook to excursions in the Vienna Basin and the adjacent Alpine-Carpathian thrustbelt in Austria: *Mitt. Oesterr. Geol. Ges.*, v. 85, p. 1-264.
- Schroeckenfuchs, G., 1975, Hydrogeologie, Geochemie und Hydrodynamik der Formationswässer des Raumes Matzen - Schoenkirchen Tief. *Erdöl-Erdgas Zeitschrift* 91, p. 299-321.
- Seifert, P., 1996, Sedimentary-tectonic development and Austrian hydrocarbon potential of the Vienna Basin. In: Wessely, G. and Liebl, W. (Eds.): *Oil and gas in Alpidic thrustbelts and basins of central and eastern Europe: EAGE Spec. Publ.* v. 5, p. 331-341.
- Shipton, Z. K. and Cowie, P.A., 2001, Damage zone and slip-surface evolution over μm to km scales in high-porosity Navajo sandstone, Utah: *Journal of Structural Geology*, v. 23, p. 1825-1844.
- Steininger, F. and G. Wessely, 2000, From the Tethyan Ocean to the Paratethys Sea: Oligocene to Neogene stratigraphy, paleogeography and paleobiogeography of the circum-Mediterranean region and the Oligocene to Neogene basin evolution in Austria. *Mitt. Oesterr. Geol. Ges.*, v. 92, p. 95-116.
- Sternlof, K. R., M. Karimi-Fard, D.D. Polard and L.J. Durlofsky, 2006, Flow and transport effects on compaction bands in sandstone at scales relevant to aquifer and reservoir management: *Water Resources Research*, v. 42, issue: W07425, p. doi:10.1029/2005WR004664.
- Strauss, P., M. Harzhauser, R. Hinsch, and M. Wagreich, 2006, Sequence stratigraphy in a classic pull-apart basin (Neogene, Vienna Basin). A 3D seismic based integrated approach: *Geologica Carpathica* v. 57, p. 185-197.
- Wagreich, M. and H.P. Schmid, 2002, Backstripping dip-slip fault histories: apparent slip rates for the Miocene of the Vienna Basin: *Terra Nova* v. 14, p. 163-168.
- Weissenbaeck, M., 1996, Lower to Middle Miocene sedimentation model of the central Vienna Basin. In: Wessely, G. and Liebl, W., (Eds.): *Oil and gas in Alpidic thrustbelts and Basins of the Central and Eastern Europe: EAGE Spec. Publ.* 5, p. 355-363.

Wessely, G., 1988, Structure and development of the Vienna basin in Austria. In: Royden L. and Horvath F. (Eds.): The Pannonian basin. A study in basin evolution: AAPG, v. 45, p. 333-346.

Appendix

Additional results

X- ray diffraction measurements were made to compare the mineralogical composition of host rock and deformation bands (Figure 21 and Figure 22). Core samples from a well taken at a depth of 1651m show a difference in the mineralogical composition. This sample does not contain clay minerals, as muscovite, chlorite and kaolinite in the deformation band. Samples from depths of 1647.3m, 1649.3m and 1656.5m do not show a significant difference in mineralogical composition.

In addition BSE images and element maps were analyzed in order to identify potential grain size reductions. The silica element maps highlight feldspar, mica (gray-yellow) and quartz grains (light yellow). The magnesium and calcium element maps show the distribution of detrital dolomite grains and dolomite cement. The iron and sulfur element maps indicate pyrite while potassium and aluminum highlight K-feldspar (Figure 23, Figure 24 and Figure 25).

The chemical composition of detrital dolomite grains was measured by single point analyses with the electron microprobe. The quantitative measurements show a significant difference in FeO concentration between detrital grains and dolomite cement. The dolomite cement has a content of 10-12 wt% FeO, whereas the host rock has only 0-2wt% FeO (Table1).

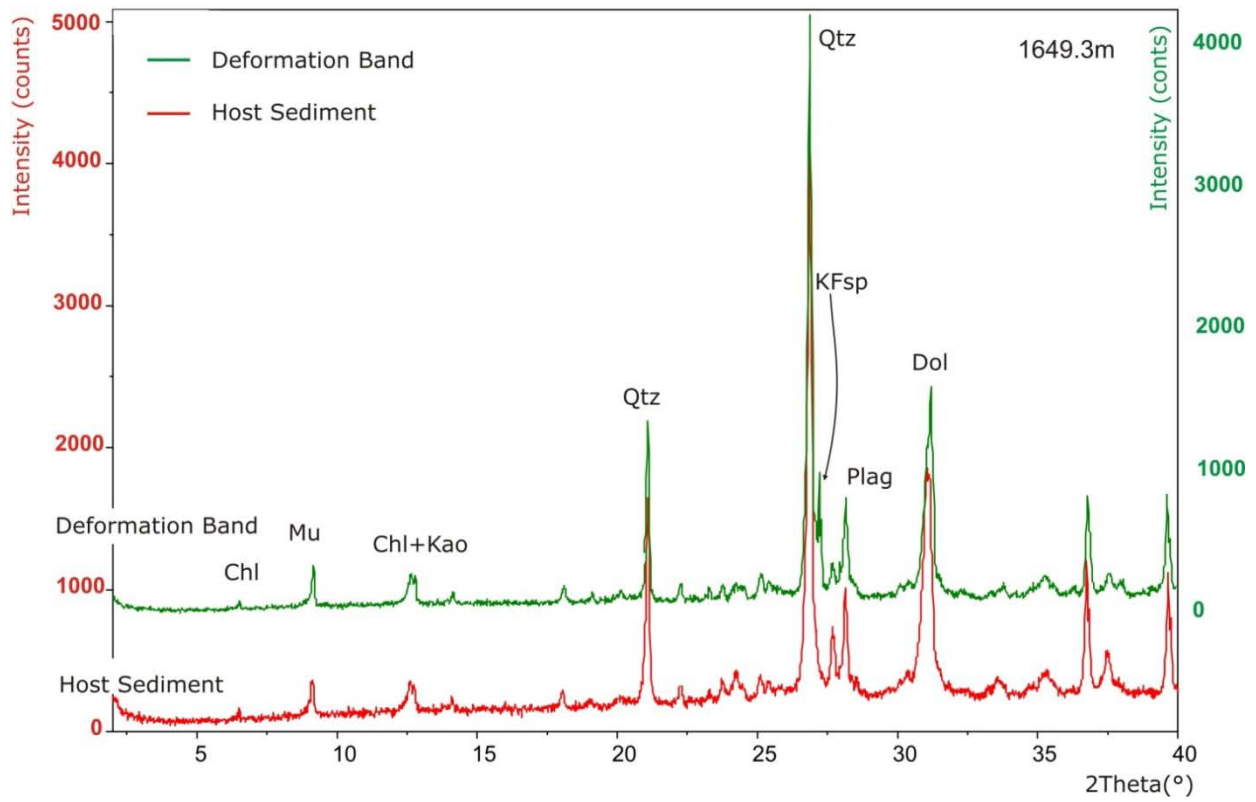
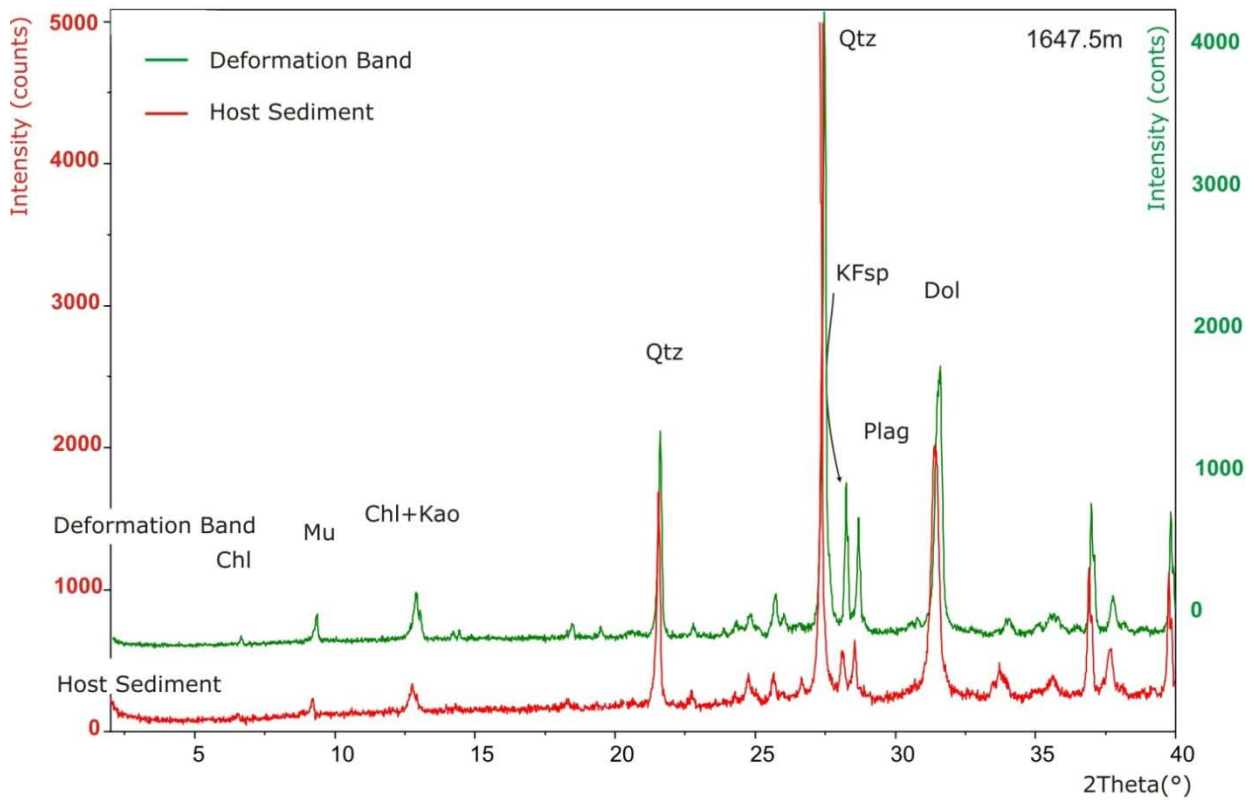


Figure 21: X-ray diffraction pattern, mineralogical composition of deformation band and the host sediment of the samples 1647.5m and 1649.3m (Chl=chlorite, Mu=muscovite, Kao=kaolinite, Qtz=quartz, KFs=K-feldspar, Plag=plagioclase, Dol=dolomite)

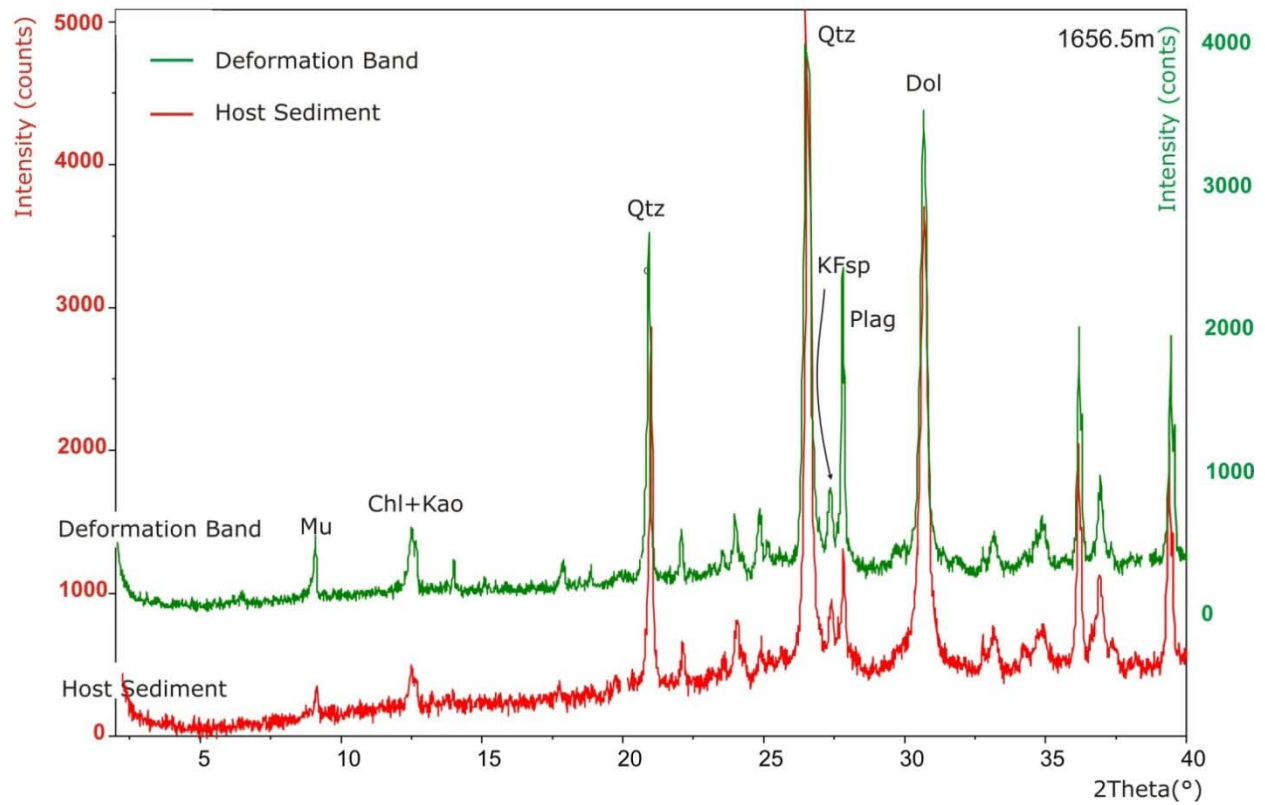
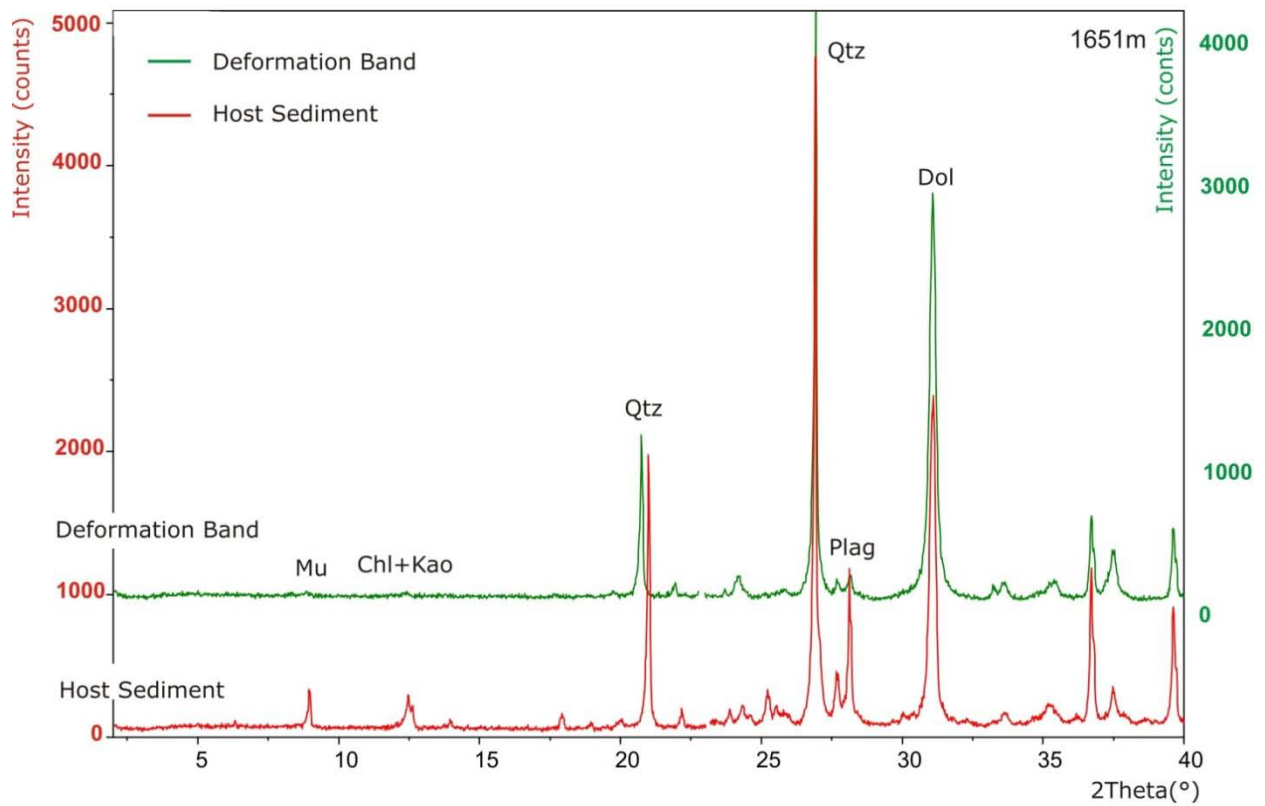


Figure 22: X-ray diffraction pattern, mineralogical composition of deformation band and the host sediment of the samples 1651m and 1656.5m (Chl=chlorite, Mu=muscovite, Kao=kaolinite, Qtz=quartz, KFsp=K-feldspar, Plag=plagioclase, Dol=dolomite)

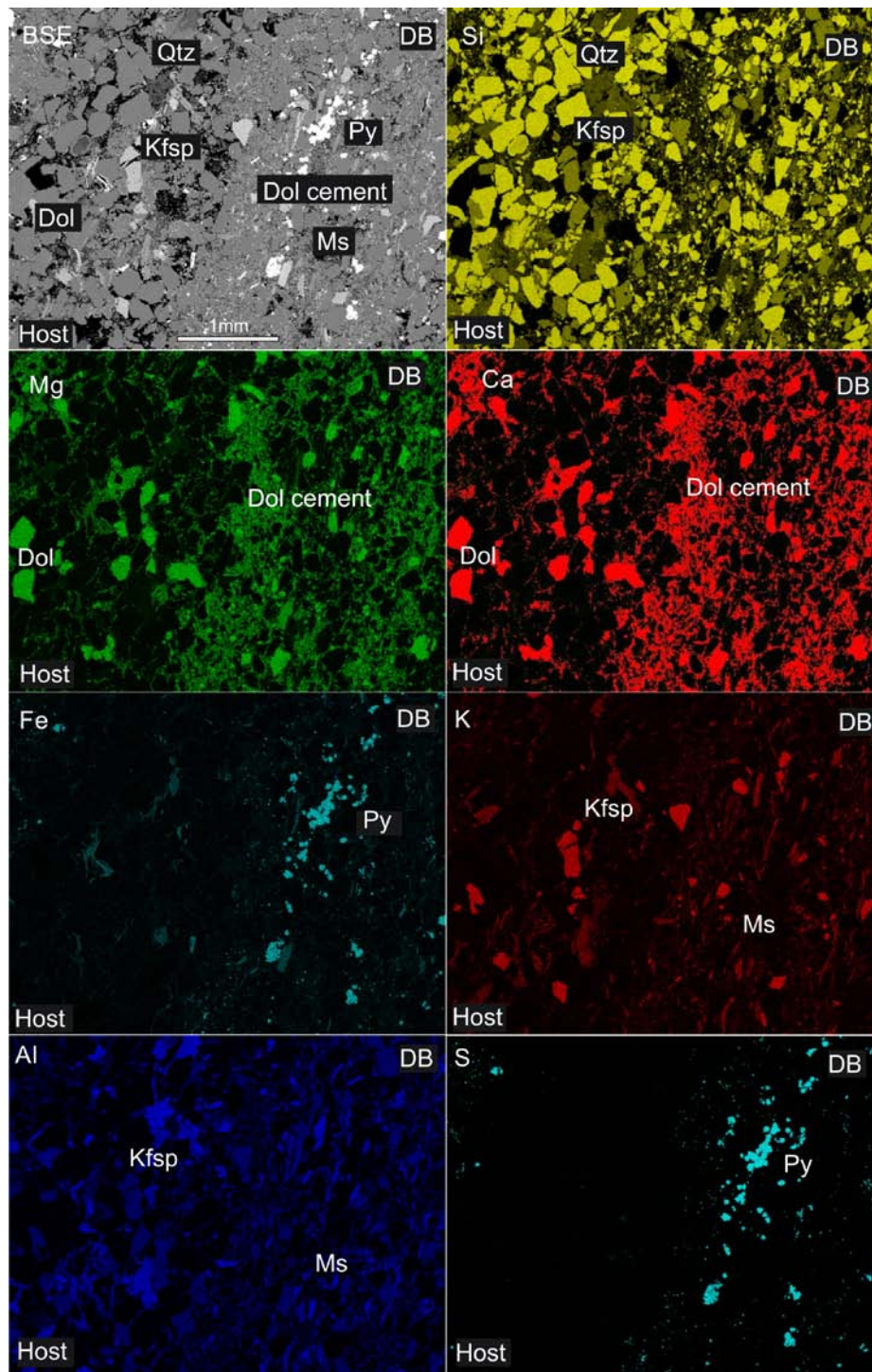


Figure 23: BSE image of sample 1651m showing the deformation band on the right and the host rock on the left; element map of Si showing K-feldspar (gray-yellow) and quartz grains (light yellow); the Mg and Ca images display the dolomite cement and detrital dolomite grains in both host rock and deformation band; Fe image highlight pyrite and the Fe rich dolomite cement (gray blue); the K and Al images indicate K-fsp and muscovite.

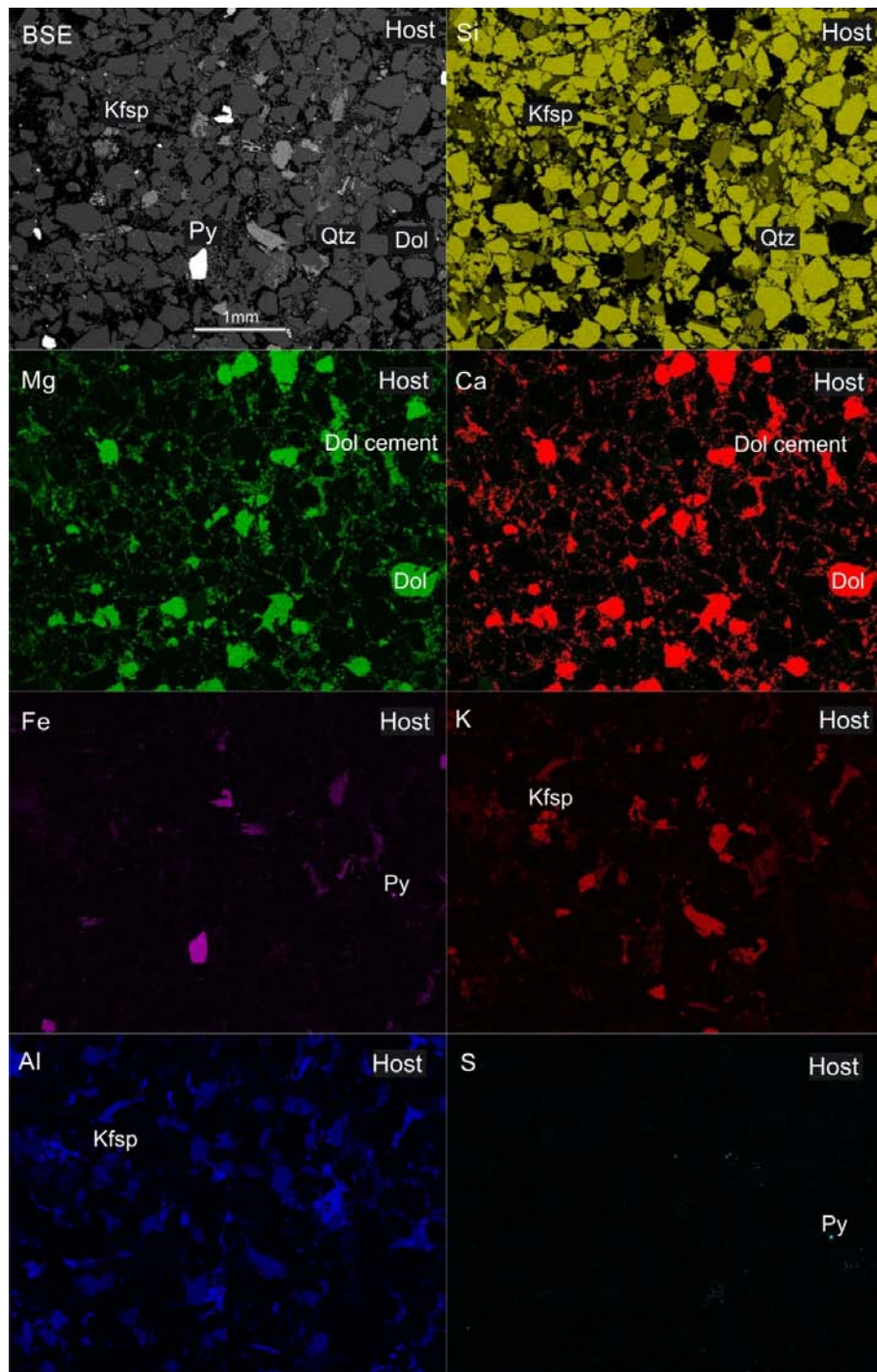


Figure 24: BSE image of sample 1656.5m showing the host rock; element map of Si showing K-feldspar (gray-yellow) and quartz grains (light yellow); the Mg and Ca images display the detrital dolomite grains and dolomite cement; the Fe and S images highlight pyrite; the K and Al images indicate K-fsp and muscovite.

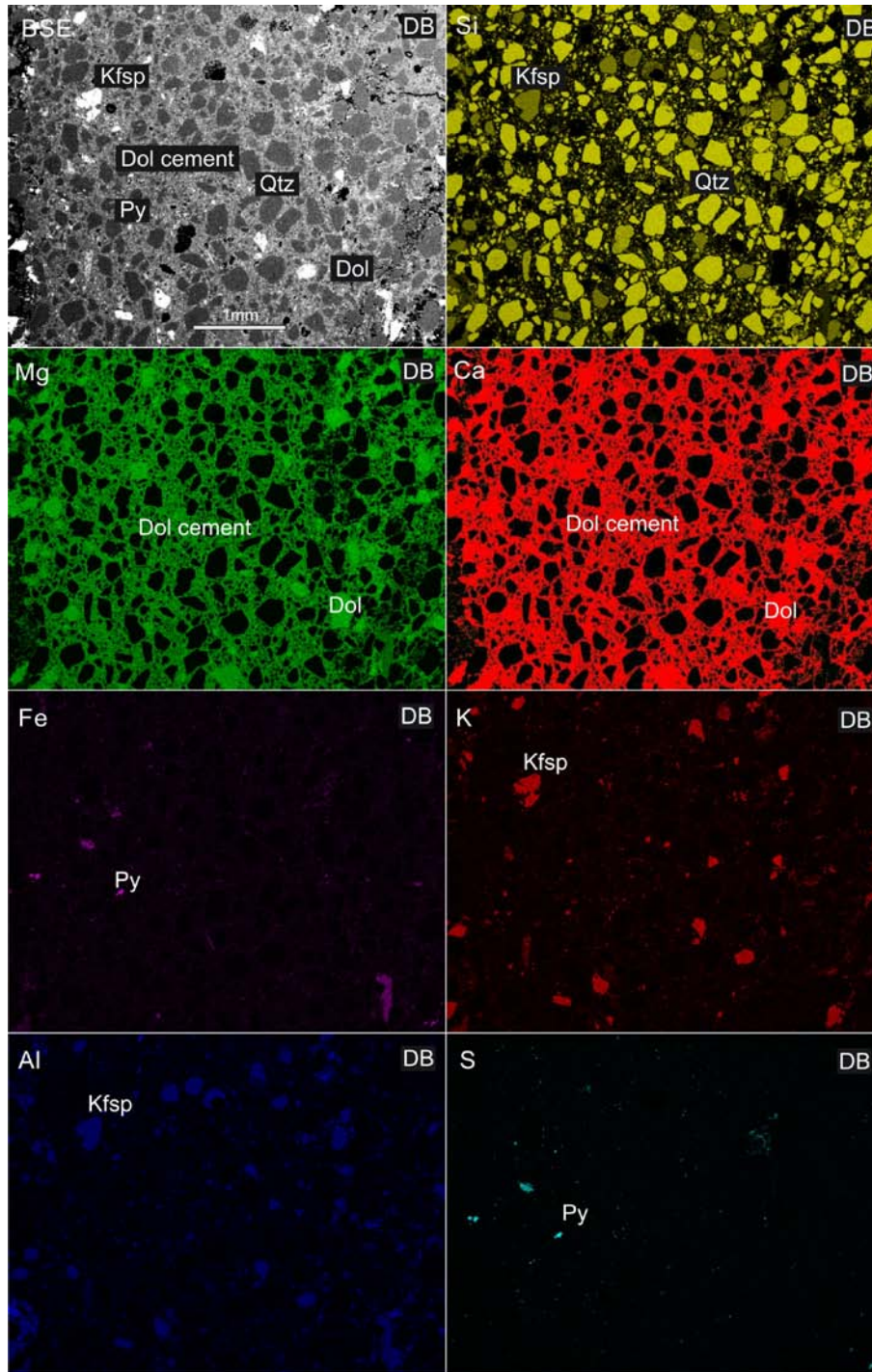


Figure 25: BSE image of sample 1656.5m showing the deformation band; element map of Si showing feldspar (gray-yellow) and quartz grains (light yellow); the Mg and Ca images display the dolomite cement and detrital dolomite grains; the Fe image highlight pyrite and the Fe rich dolomite cement (gray-blue); the K and Al images indicate K-fsp and muscovite; the S image shows pyrite.

Single point analyses of detrital dolomite grains and dolomite cement

DataSet/Point	Na2O	MgO	Al2O3	SiO2	CaO	K2O	FeO	MnO	Total	Comment	Grain/Cements
1 / 1 .	0	12.79	0.09	0.3	31.07	0.02	11.56	0.14	55.96	1651_a_009_pt1	Cement
2 / 1 .	0.04	10.12	1.2	17.8	25.76	0.16	9.59	0.06	64.74	1651_a_009_pt2	Cement
3 / 1 .	0	12.23	0.76	1.23	30.71	0.07	11.68	0.1	56.79	1651_a_009_pt3	Cement
4 / 1 .	0.21	20.65	0.05	0.17	31.98	0.01	1.41	0.41	54.9	1651_a_009_Line1	Grain
4 / 2 .	0.03	20.5	0	0.16	30.42	0.01	2.46	0.56	54.13	1651_a_009_Line1	Grain
4 / 3 .	0	20.4	0.02	0.06	30.21	0.01	2.43	0.54	53.67	1651_a_009_Line1	Grain
4 / 4 .	0	20.47	0.02	0.05	30.56	0	2.49	0.55	54.14	1651_a_009_Line1	Grain
4 / 5 .	0.01	20.8	0.01	0.08	30.12	0	2.57	0.59	54.17	1651_a_009_Line1	Grain
4 / 6 .	0.02	20.4	0.02	0.06	30.49	0.01	2.57	0.65	54.23	1651_a_009_Line1	Grain
4 / 7 .	0	20.55	0.07	0.1	30.3	0	2.61	0.56	54.18	1651_a_009_Line1	Grain
4 / 8 .	0.14	20.16	0.11	0.19	31.26	0	1.75	0.42	54.02	1651_a_009_Line1	Grain
5 / 1 .	0.04	19.44	0.19	0.26	32.02	0.03	1.91	0.27	54.16	1651_a_009_Line2	Grain
5 / 2 .	0	20.4	0.03	0.11	30.18	0.01	2.61	0.56	53.89	1651_a_009_Line2	Grain
5 / 3 .	0.01	20.71	0.01	0.11	31.11	0	2.61	0.55	55.12	1651_a_009_Line2	Grain
5 / 4 .	0	20.65	0	0.07	30.04	0.01	2.52	0.53	53.82	1651_a_009_Line2	Grain
5 / 5 .	0	20.58	0.03	0.08	30.36	0	2.7	0.6	54.35	1651_a_009_Line2	Grain
5 / 6 .	0.07	20.58	0.07	0.12	30.62	0	2.28	0.7	54.43	1651_a_009_Line2	Grain
6 / 1 .	0.14	20.89	0.11	0.13	32.11	0	0.76	0.23	54.37	1651_a_009_pt4	Grain
7 / 1 .	0.19	20.79	0.13	0.35	32.22	0.02	1.18	0.43	55.3	1651_a_009_pt5	Grain
8 / 1 .	0.01	22.22	0.05	0.14	31.85	0.04	0.13	0	54.44	1651_a_009_pt6	Grain
9 / 1 .	0.18	20.13	0.7	1.41	31.53	0.15	1.01	0.28	55.39	1651_a_009_pt7	Grain
10 / 1 .	0.15	20	0.39	1.05	32.49	0.11	0.66	0.21	55.07	1651_a_009_pt8	Grain
11 / 1 .	0.03	22.24	0.03	0.06	33.33	0.01	0.12	0.02	55.83	1651_a_009_pt9foc	Grain
12 / 1 .	0.03	20.2	0.01	0.07	35.1	0.04	0.4	0.01	55.87	1651_a_009_pt10	Grain
13 / 1 .	0.03	22.04	0.04	0.09	33.01	0.04	0.11	0.02	55.36	1651_a_009_pt9def	Grain
14 / 1 .	0.21	20.1	0.4	1.17	31.63	0.1	1.33	0.27	55.21	1651_a_009_pt11	Grain
15 / 1 .	0.02	22.7	0	0.08	31.95	0	0.06	0.02	54.83	1651c_pt12	Grain
16 / 1 .	0.03	22.38	0.03	0	31.81	0	0.05	0	54.3	1651c_pt13	Grain
17 / 1 .	0	0	0.01	99.26	0.16	0	0.07	0.01	99.52	1651c_pt14	Grain
18 / 1 .	0.01	22.6	0.01	0.04	31.43	0.02	0.03	0	54.14	1651c_pt15	Grain
19 / 1 .	0.08	20.36	0.1	0.8	33.54	0.06	0.33	0.21	55.46	1651c_pt16	Grain
20 / 1 .	0.21	20.03	0.77	2.39	30.93	0.18	1.21	0.29	56.01	1651c_pt17	Grain
21 / 1 .	0.18	19.39	0.86	1.87	30.78	0.18	1.36	0.34	54.96	1651c_pt18	Grain
22 / 1 .	0.01	22.93	0.04	0.11	31.95	0.01	0.06	0.02	55.14	1651c_pt19	Grain
23 / 1 .	0.01	22.46	0.02	0.13	31.51	0.04	0.05	0.03	54.26	1651c_pt20	Grain
24 / 1 .	0.01	20.51	0.03	0.12	33.36	0.04	0.71	0.06	54.85	1651c_pt21	Grain
25 / 1 .	0	19.73	0.06	0.02	33.05	0.01	1.05	0.14	54.06	1651c_pt22	Grain
26 / 1 .	0.08	19.52	0.08	0.24	35.27	0.03	0.15	0.03	55.41	1651c_pt23	Grain
27 / 1 .	0	11.57	0.12	0.71	31.24	0.01	12.14	0.12	55.91	1651c_pt24	Cement
28 / 1 .	0.02	9.41	0.95	14.44	25.39	0.25	10.38	0.1	60.94	1651c_pt25	Cement
29 / 1 .	0.18	20.54	0.09	0.28	32.64	0.04	0.74	0.29	54.81	1651c_pt29	Grain
30 / 2 .	0.01	22.57	0	0.03	31.72	0	0.02	0	54.35	1651c_pt27_average	Grain
30 / 3 .	0	22.26	0.01	0.03	31.38	0.01	0.07	0	53.77	1651c_pt27_average	Grain
30 / 4 .	0	22.66	0.01	0.04	31.49	0	0.03	0	54.22	1651c_pt27_average	Grain
31 / 1 .	0.05	20.54	0.49	0.92	32.77	0.09	0.42	0.25	55.54	1651c_pt30	Grain

Table 1: Single point analyses display a significant difference in FeO content. Dolomite cement contain 10-12wt% FeO in contrast to detrital dolomite grains with 0-3wt%.

Acknowledgment

First of all I want to thank my advisors Mag. Dr. Ulrike Exner and Ao. Univ.-Prof. Mag. Dr. Susanne Gier for their extensive support, guidance and advice during my work on my master thesis. Without their encouragement this thesis could not have been done.

For providing the samples the OMV AG and particularly Mag. Philipp Strauß, Dr. Roman Sauer and Mag. Wolfgang Hujer have to be thanked, and especially for their expert knowledge.

Further I want to thank Hugh Rice and Christian Baal for their help with the Scanning Electron Microscope. For the help with the Cathodoluminescence I want to thank Dieter Mader, as well as Franz Kiraly who assisted me in using the electron microprobe.

To my colleagues Johannes Steinbrener, Clemens Porpaczy, Bernhard Bretis, Andrea Schicker, Angelika Kern and Alexander Rath my most sincere thanks for their advice, time, patience and support during my master studies.

Special thanks to Mischo Erban for always listening to my complaints, the time he spent proofreading and encouraging me whenever I lost motivation or focus.

I also want to thank my parents for their great support, their patience and trust in me during my entire education. Without their support my studies would not be possible.

CURRICULUM VITAE

Personal Data:

Name: Jasmin-Corin Kaiser
Academic degree: Bakk. rer. nat.
Born on: 22.01.1986
Born in: Vienna
Nationality: Austria
Permanent Address: A-1210 Vienna
Ostmarkgasse 48/2/3
Email: jasmincorinkaiser@gmx.at

Education:

09/1996 – 06/2004 Highschool: BG&BRG Franklinstrasse, Vienna

10/2004 – 06/2005 University of Leoben
Undergraduate student in Applied Geosciences

10/2005 – 12/2008 University of Vienna
Bachelor study in Earth Sciences

 Bachelor Thesis: “Grain size and grain shape of gravels in Miocene delta sediments with deformation bands”

12/2008 – 11/2011 University of Vienna
Master study in Geology

 Master Thesis: "Microstructures and mineralogy of deformation bands in drill cores from the Matzen hydrocarbon reservoir" in cooperation with OMV

Academic Employment:

2009 WS Tutor for introductory geology at the University of Technology in Vienna
2010 SS Tutor for geological mapping and methods at the University of Vienna
2011 WS Tutor for introductory geology at the University of Technology in Vienna
2011 WS Tutor for Sedimentology at the University of Vienna
2011 SS Tutor for geological mapping and methods at the University of Vienna

Summer Internship:

07/2002 IBM: Data processing and IT – Support, Vienna
07/2003 IBM: Data processing and IT – Support, Vienna
08/2004 Side By Side Consulting: IT-Support, Vienna
07/2007 OMV: Department Operation Geology, Vienna
07/2008 OMV: Department Geological Laboratory, Vienna
07/2009 OMV: Department Operation Geology, Vienna
07/2010 OMV: Department Geological Laboratory, Gänserndorf

Languages:

German (mother tongue), English (fluent), French (basic), Italian (basic)

Published Abstracts:

Tuitz, C., Exner, U., Grasemann, B., Kaiser, J., Seidl, S., Preh, A., Gier, S., Wagneich, M. (2008) The influence of grain size distribution on contact stresses acting between pebbles in unconsolidated gravel layers. Pangeo Austria 2008, 23.-24. September 2008, Abstract Volume, Mitteilungen der Gesellschaft der Geologie- und Bergbaustudenten in Österreich, 49.

Kaiser, J., Exner, U., Gier, S., Hujer, W. (2010) Porosity and permeability reduction along deformation bands in a hydrocarbon reservoir (Matzen, Austria). EGU Austria 2010, EGU2010-4196.

Kaiser, J., Exner, U., Gier, S., Hujer, W. (2010) Microstructures and mineralogy of deformation bands in drill cores from the Matzen hydrocarbon reservoir (Austria), Pangeo Austria 2010.

Kaiser, J., Exner, U., Gier, S., Hujer, W. (2011) Preferred cementation by iron rich dolomite along deformation bands in a hydrocarbon reservoir, Matzen, (Austria). EGU Austria 2011, EGU2010-4196.